FOREWORD

This report presents the results of a portion of the experimental program for an investigation of hypersonic flow separation and control characteristics conducted by the Research Department of Grumman Aircraft Engineering Corporation, Bethpage, New York. The work was partly sponsored by the Flight Dynamics Laboratory, Research and Technology Division, Wright-Patterson Air Force Base, Ohio, under Contract AF33(616)-8130, Air Force Task 821902. Mr. Donald E. Hoak was the Air Force Project Engineer for the program.

ABSTRACT

This report presents heat transfer and pressure distributions for hypersonic flows ahead of ramps, over expansion corners, and past fin-plate combinations. Two basic models were used for these experiments: 1) a flat plate with a full span ramp (trailing-edge flap) on one surface and an expansion corner on the other, and 2) a flat plate with wedge shaped fins mounted on the upper surface and an expansion corner on the lower surface. Both sharp leading edge models were tested in the Grumman Hypersonic Shock Tunnel at Mach 13 and 19. The plate-flap model was tested at $\alpha = -15°$ to $+30°$, with flap deflections from $0°$ to $45°$, at Reynolds numbers per foot of 0.8×10^5 to 1.4×10^5 at Mach 19 and of 1.2×10^5 at Mach 13. The fin-plate model was tested at $\alpha = 0$ only, with 15 degree wedge shaped fins having two different heights at a Reynolds number per foot of 2.4×10^5 at Mach 13 and of 0.8×10^5 at Mach 19.

This technical documentary report has been reviewed and is approved.

for C. R. Bryan
W. A. SLOAN, Jr.
Colonel, USAF
Chief, Flight Control Division
AF Flight Dynamics Laboratory

TABLE OF CONTENTS

LIST OF ILLUSTRATIONS

LIST OF ILLUSTRATIONS (Cont)

LIST OF ILLUSTRATIONS (Cont)

LIST OF TABLES

LIST OF SYMBOLS

C_p	pressure coefficient, $C_p \equiv (p - p_\infty) / q_\infty$
h	heat transfer coefficient (BTU/ft^2 sec °R), $h \equiv \dot{q}_w/(T_o - T_w)$
k_∞	thermal conductivity of free stream flow (BTU/ft sec °R)*
M_∞	free stream Mach number*
Nu	Nusselt number, $Nu \equiv hx/k_\infty$
p	pressure (psia)
p_o	stagnation pressure (psia)
p_∞	free stream static pressure (psia)*
$\dot{q}_w$	aerodynamic heating rate (BTU/ft^2 sec)
q_∞	free stream dynamic pressure (psia)*
Re_x	local Reynolds number $Re_x \equiv \rho_\infty U_\infty x/\mu_\infty$
Re_∞/ft	free stream Reynolds number per foot, $Re_\infty/ft \equiv \rho_\infty U_\infty/\mu_\infty$*
S	nondimensional streamwise distance
S_u	upper surface streamwise distance
S_ℓ	lower surface streamwise distance
t	time (sec)
T_o	stagnation temperature (°R)

LIST OF SYMBOLS (Cont)

T_w	wall temperature (°R)
T_∞	free stream static temperature (°R)*
U_∞	free stream velocity (ft/sec)*
x, y, z	coordinate axes defined in Figs. 2 and 4
μ_∞	free stream viscosity (slugs/ft sec)
ρ_∞	free stream density (slugs/ft^3)

*Free stream properties are calculated at the leading edge model station.

INTRODUCTION

The Grumman Research Department has been investigating hypersonic flow separation and the effectiveness of controls in separated flow zones. The experimental effort involved testing four basic configurations in the Arnold Engineering Development Center (AEDC) Tunnels A, B, and Hotshot 2, as well as in the Grumman Hypersonic Shock Tunnel (GHST). Eleven distinct models were built in order to accommodate pressure, heat transfer, and force measurements as well as to meet the requirements of the various facilities. Sketches of the configurations, along with some pertinent remarks for the over-all program, are shown in Fig. 1. The four basic configurations are labeled A, B, C, and D. Configurations A and B were designed primarily to study flow separation, while configurations C and D were designed primarily to provide controls information for typical hypersonic flight configurations. Detailed design information and test plans are given in Ref. 1.

This report deals with configurations A and B and presents pressure and heat transfer data that were obtained in the Grumman Hypersonic Shock Tunnel at nominal Mach numbers 13 and 19 during early 1964. The models in this tunnel entry are one half scale of the ones that were tested at Mach numbers 5 and 8 at AEDC.

The purpose of the tests reported here is twofold: first to generate experimental information at Mach 13 and 19, and second to provide possible guidelines for extending the Mach 5 and 8 data to higher Mach numbers. Results for the over-all program will be presented in a forthcoming final report. Two runs were made using Krylon white enamel as a heat sensitive paint and the results are discussed briefly. Schlieren photography was employed and some typical photographs are presented.

Manuscript released by the author August 1964 for publication as an FDL Technical Documentary Report.

MODELS

Dimensions, pressure tap, and thermocouple locations as well as coordinate axes definitions for model A are given in Fig. 2. Instrumentation coordinates are given in Table I. Model A has a six-inch square planform and a nominally sharp leading edge (35° included angle). The upper surface was designed for the study of the flow ahead of ramps and the lower surface for the study of the flow over 40° expansion corners. The trailing edge flap is of 25 per cent chord and is shown in Fig. 2 for the three flap settings studied in this tunnel entry.

Model B is pictured in Fig. 3; dimensions, instrumentation locations, and coordinate axes definitions are given in Fig. 4. Instrumentation coordinates are given in Table II. The body of model B has a six-inch square planform with a trapezoidal profile and is one and one half inches deep. The lower face of the body intersects the upper surface forming an angle of 30° at the leading edge. The leading edge of the model and the 30° expansion corner on the lower surface are machined sharp. A small, sharp leading edge fin is mounted symmetrically about the centerline on the flat plate upper surface of the model. The wedge shaped fin has a semi-vertex angle of 15°. An attachable fin portion provides an extra fin configuration of 2-inch height.

TEST CONDITIONS

Model A was tested at angles of attack of -15° to +30°, referenced to the upper flat plate surface. The convention used here is that compression of the upper surface indicates positive angles of attack. Model B was tested only at zero angle of attack, also referenced to the upper flat plate surface. The flap deflections for model A were 0, 15°, 30°, and 45°; model B was tested with two wedge fins separately.

Both models were run at nominal Mach numbers of 13 and 19. The range of free stream Reynolds number per foot was from 0.8×10^5 to 2.4×10^5. A detailed presentation of the test program and corresponding test conditions are shown in Table III. A number of runs were repeated and are so indicated in the table.

The free stream conditions shown in Table III are those obtained at the leading edge of the model. These conditions are

not duplicated exactly from run to run and are thus indicated in the table. Useful test flow durations of approximately 3 milliseconds were obtained for these conditions. Further, because the GHST has a conical nozzle, the free stream conditions vary in the test section along the tunnel centerline. Distributions of the free stream static pressure, temperature, and Mach number along the tunnel centerline are plotted versus axial distance downstream of the nozzle exit in Figs. 5 and 6. A more detailed description of the facility is given in Ref. 3.

DATA REDUCTION AND ACCURACY

Pressure and heat transfer data were reduced to the standard coefficient forms presented herein by using reference "free stream" conditions. These were taken as those at the leading edge of the models.

Measured pressures p were reduced to pressure coefficients,

$$C_p = \frac{p - p_\infty}{q_\infty}$$

using the reference free stream values of the static and dynamic pressures, p_∞ and q_∞.

Aerodynamic heating rates $\dot{q}_w$ were presented directly by the heat transfer gauge instruments (from measurements of the transient wall temperatures T_w). The heating rates were nondimensionalized in the form

$$\frac{Nu}{\sqrt{Re_x}} = \left(\frac{\dot{q}_w}{T_o - T_w}\right)\left(\frac{x}{k_\infty}\right)\sqrt{\frac{\rho_\infty U_\infty x}{\mu_\infty}}$$

where Nu is the Nusselt number, x is the streamwise distance from the leading edge to the heat transfer gauge* (see Figs. 2 and 4), and Re_x is the Reynolds number based on distance x.

---

*For model A, x is the running length at all flap settings while for model B, x is a projected length.

For each test run, the values of k_∞, ρ_∞, U_∞, and μ_∞ (the thermal conductivity, density, velocity and viscosity of the free stream flow respectively), were calculated at the model's leading edge station. Values of k_∞ and Re_∞/ft are given in Table III for each test run. For the low temperature encountered in these tests, the conductivity k_∞ was calculated by assuming a Prandtl number equal to 0.73, a specific heat at constant pressure $c_p = 0.24$ BTU/lbm °R, and a viscosity dependence $\mu = \frac{2.21\ T^{3/2}}{T + 178.6} \times 10^{-8}$ slugs/ft sec.

Pressures were estimated to be accurate to within 10 per cent of their measured values. In addition to these estimates, the data on the lower surface of both models provide a certain degree of repeatability, since the flow there should not be influenced by geometrical changes on the upper surface. The accuracy for the heating rates is not as good as for the pressures. This is to be expected for a facility of small duration testing time. The repeatability in most cases is good and within a 10 per cent range. In some instances, and particularly in the interaction zone of model B, repeatability of less than 10 per cent was not always obtained. This might very well be due to the sensitivity of the corner flow and not necessarily to instrumentation defects. Occasionally the oscilloscope trace of a point was very "noisy" and difficult to read. Such points have been omitted in the presentation of the data. Lastly, we mention that artificial errors may be introduced in the process of nondimensionalizing the data, since the free stream conditions can very well vary.

PRESENTATION OF RESULTS

The presentation of the data differs distinctly for the two models. For model A the pressure and heat transfer rates are plotted versus a nondimensionalized streamwise distance S. For the upper surface, the parameter S_u is defined as the ratio of the chordwise surface distance of a point from the leading edge of the model to the surface length of the model. For the lower surface, the parameter S_ℓ is defined as the ratio of the chordwise surface distance of a point from the expansion corner to the true length of the model aft of the expansion corner. With this artifice we have presented the data for both the upper and lower surfaces on the same graph page.

For model B we have presented the data at two chordwise stations versus the semispan Y and wedge height Z. The Nusselt number for this model is based on the x projection of a point. There is a degree of arbitrariness in using the projection, especially for the wedge, and we do not attribute any physical significance to this presentation.

The data for model A are presented in Figs. 7 through 22; those for model B in Figs. 23 through 30. The symbols are defined in the figures. Whenever a run was repeated the symbols are flagged, and filled symbols are used whenever the Reynolds number per foot was higher than 10^5. Schlieren photographs were obtained throughout the program; some are presented in Figs. 31, 32, and 33.

In Ref. 2 we reported on the use of Krylon white enamel as a heat sensitive paint and recommended its use for preliminary, qualitative investigations of complicated configurations, which have many areas of interaction. A winged re-entry configuration was tested in the AEDC Hotshot 2 tunnel and clearly defined regions of increased aerodynamic heating were observed. Two runs were made in the present test series using the Krylon white enamel paint. Photographs of model A before and after the run and model B after the run are presented in Figs. 34, 35, and 36. Although hot areas can be seen in these pictures, there exists a lack of detail, which can be attributed in part to the considerably shorter duration of the GHST test runs. The use of Krylon is best employed for preliminary analyses of complicated configurations in test facilities having longer test durations.

REFERENCES

1. Evans, W. J., and Kaufman, L. G. II, Pretest Report on Hypersonic Flow Separation and Control Models for AEDC Tunnels A, B, Hotshot 2 and Grumman Hypersonic Shock Tunnel, Grumman Research Department Memorandum RM-209, July 1962.

2. Hartofilis, S. A., Pressure Measurements at Mach 19 for a Winged Re-entry Configuration, ASD-TDR-63-319, May 1963.

3. Hopkins, H. B., Scheuing, R. A., and Leng, J., Investigation of Pressure Distributions over Planar, Twisted and Cambered Wings in a Hypersonic Shock Tunnel, ASD-TDR-62-171, May 1962.

4. Wallace, A. R., and Swain, W. N., Pressure Distribution Tests on a 60° and 70° Delta Wing at Mach Numbers 20 to 22, AEDC-TN-61-14, February 1961, CONFIDENTIAL REPORT.

5. Kaufman, L. G. II, Pressure and Heat Transfer Measurements for Hypersonic Flows Over Expansion Corners and Ahead of Ramps, ASD-TDR-63-679, Part I: Mach 5 and 8 Data for Expansion Corner Flows, September 1963, Part II: Mach 5 Pressure Data for Flows Ahead of Ramps, September 1963, Part III: Mach 8 Pressure Data for Flows Ahead of Ramps, December 1963, Part IV: Mach 8 Heat Transfer Data for Flows Ahead of Ramps, to be published.

6. Baer, A. L., An Investigation of Separated Flows on Two-Dimensional Models at Mach Numbers 5 and 8, AEDC-TDR-63-200, October 1963.

7. Burchfield, C. G., Hube, F. K., and Burdette, J. E., An Experimental Heat-Transfer Investigation in Regions of Flow Separation at Mach Number 8, AEDC-TDR-64-30, February 1964.

8. Kaufman, L. G. II, Pressure Measurements for Mach 8 Flows Over Expansion Corners and Ramps on an Internally Cooled Model, RTD-TDR-63-4044, Part I: Expansion Corner Flows, October 1963, Part II: Flows Over a Flat Plate with and without a Partial Span Ramp, to be published, Part III: Flows Over Full Span Ramps Mounted on a Flat Plate, to be published.

9. Kaufman, L. G. II, and Meckler, L. H., Pressure and Heat Transfer Measurements at Mach 5 and 8 for a Fin - Flat Plate Model, ASD-TDR-63-235, April 1963.

10. Kaufman, L. G. II, Pressure Distributions and Oil Film Photographs for Mach 5 Flows Past Fins Mounted on a Flat Plate, ASD-TDR-63-755, September 1963.

11. Kaufman, L. G. II, Pressure Measurements for Mach 5 Flows Over Winged Re-entry Configurations with Aerodynamic Controls, RTD-TDR-63-4179, Part I: Blunt Cabin Configuration, February 1964, Part II: Conical Cabin Configuration, February 1964.

12. Meckler, L., Pressure Measurements at Mach 8 on an Aerodynamically Controllable Winged Re-entry Configuration, to be published as an FDL Technical Documentary Report.

13. Meckler, L., Heat Transfer Measurements at Mach 8 on an Aerodynamically Controllable Winged Re-entry Configuration, to be published as an FDL Technical Documentary Report.

14. Donaldson, J. C., Hypersonic Control Effectiveness Tests of a Delta-Winged Re-entry Configuration at Mach 5 and 8, AEDC-TDR-63-268, December 1963.

15. Lacey, J. J., Jr., Pressure Tests on a Blunt Delta Wing Vehicle at M = 19, AEDC-TDR-63-32, February 1963.

16. Meckler, L., Static Aerodynamic Characteristics at Mach 5 and 8 for an Aerodynamic Controllable Winged Re-entry Configuration, FDL-TDR-64-10, to be published.

17. Kaufman, L. G. II, Pressure Measurements for Mach Five Flows Over a Blunt Pyramidal Configuration with Aerodynamic Controls, RTD-TDR-63-4239, January 1964.

18. Kaufman, L. G. II, Pressure and Heat Transfer Measurements for Mach 8 Flows Over a Blunt Pyramidal Configuration with Aerodynamic Controls, FDL-TDR-64-2, Part I: Pressure Data for Delta Wing Surface, January 1964, Part II: Pressure Data for Dihedral Surfaces and Part III: Heat Transfer Data for Delta Wing Surface, to be published, and Part IV: Heat Transfer Data for Dihedral Surfaces, May 1964.

19. Donaldson, J. C., Hypersonic Control Effectiveness Tests of a Blunted, Triangular-Pyramid Re-entry Configuration at Mach 5 and 8, AEDC-TDR-63-250, December 1963.

20. Evans, W. J., and Kaufman, L. G. II, Aerodynamic Characteristics and Flap Loads for a Blunt Pyramidal Configuration at Mach 5 and 8, to be published as an FDL Technical Documentary Report.

21. Kaufman, L. G. II, Pressure and Heat Transfer Measurements for Mach 21 Flows Over a Blunt Pyramidal Configuration with Aerodynamic Controls, to be published as an FDL Technical Documentary Report.

TABLE I

INSTRUMENTATION COORDINATES FOR MODEL A

Pressure Orifices			Heat Transfer Gauges		
Tap	x	y	Gauge	x	y
1	2.43	-.250	1	2.43	.500
2	2.93	-.500	2	2.93	.250
3	3.42	-.250	3	3.42	.500
4	2.688	.250	4	2.688	-.500
5	3.188	.500	5	3.188	-.250
6	3.688	.250	6	3.688	-.500
7	4.188	.500	7	4.188	-.250
8	4.750	.250	8	4.750	-.500
9	5.25	.500	9	5.25	-.250
10	5.75	.250	10	5.75	-.500

TABLE II

INSTRUMENTATION COORDINATES FOR MODEL B

Pressure Orifices

Tap	x_{in}	y_{in}	z_{in}
1	.875	0	0
2	1.375	0	↓
3	1.875	0	
4	3.000	.462	
5	3.000	.900	
6	3.000	1.650	
7	4.500	.862	
8	4.500	1.300	0
9	3.000	- .400	-1.500
10	3.250	.400	-1.500
11	3.000	.26	.312
12	4.500	.67	.312
13	3.000	.26	.937
14	4.500	.67	.937
15	4.500	.67	1.437

Heat Transfer Gauges

Gauge	x_{in}	y_{in}	z_{in}
1	1.875	.900	0
2	1.875	- .900	↓
3	3.000	- .462	
4	3.000	- .900	
5	3.000	-1.650	
6	4.500	- .867	↓
7	↓	-1.300	0
8		- .67	.312
9	↓	- .67	.937
10	4.500	- .67	1.437

TABLE III

PROGRAM SUMMARY AND TEST CONDITIONS FOR MODEL A

Run No.	α deg	δ deg	M	Re/ft x 10^{-5}	T_{o_R}	T_{∞} R	P_{∞} x 10^{4}	ρ_{∞} x 10^{7}
1254	0	30	13.73	1.19	3650	105.43	18.16	14.47
1255	0	↓	13.73	1.18	3495	100.25	16.72	14.01
1256	0	↓	13.73	1.18	3479	99.72	16.62	14.00
1409	-15	30	13.83	1.19	3170	88.42	13.94	13.24
1413	↓	0	13.83	1.21	3022	83.81	13.03	13.06
1394	↓	0	20.50	1.45	3697	48.69	4.68	8.07
1395	↓	15	↓	1.19	4660	64.84	5.90	7.64
1397	-15	30	↓	1.39	3957	52.79	5.07	8.07
1400	-15	45	20.50	1.32	4232	57.32	5.44	7.98
1265	-10	30	19.24	0.88	3517	52.08	3.33	5.37
1266	-10	30	↓	0.86	3657	54.50	3.50	5.40
1267	-10	45	↓	0.84	3791	56.84	3.66	5.41
1263	- 5	30	↓	0.87	3607	53.63	3.44	5.39
1264	↓	30	↓	0.88	3529	52.27	3.35	5.38
1281	↓	0	↓	0.84	3839	57.70	3.71	5.41
1282	- 5	0	↓	0.84	3792	56.86	3.66	5.41
1257	0	30	↓	0.87	3592	53.36	3.42	5.39
1269	↓	45	↓	0.84	3842	57.76	3.72	5.41
1270	↓	45	↓	0.85	3763	56.36	3.63	↓
1271	↓	15	↓	0.84	3849	57.88	3.73	↓
1272	↓	15	↓	0.84	3806	57.11	3.68	↓
1275	↓	0	↓	0.85	3762	56.34	3.63	5.41
1276	↓	↓	↓	0.86	3676	54.83	3.53	5.40
1380	↓	↓	19.24	1.44	3721	49.06	4.72	8.08
1382	↓	0	20.50	1.22	3918	52.16	4.37	7.03
1384	↓	15	↓	1.17	4047	54.25	4.44	6.87
1385	↓	30	↓	1.17	4109	55.27	4.58	6.97
1389	0	45	20.50	1.43	3785	50.06	4.82	8.08
1260	10	30	19.24	0.86	3646	54.31	3.49	5.40
1277	↓	0	19.24	0.85	3772	56.51	3.64	5.41
1406	↓	45	20.50	0.80	3582	50.41	2.83	4.71
1408	10	15	20.50	0.81	3473	48.65	2.72	4.69
1417	30	0	19.77	0.79	3723	52.74	2.97	4.73
1418	30	15	19.77	0.82	3357	46.78	2.60	4.66

PROGRAM SUMMARY AND TEST CONDITIONS FOR MODEL B

Run No.	α deg	Wedge	M	Re/ft x 10^{-5}	T_{o_R}	T_{∞} R	P_{∞} x 10^{4}	ρ_{∞} x 10^{7}
1451	0	Small	13.83	2.35	3334	93.64	29.97	26.88
1450	↓	Small	19.77	0.82	3373	47.05	2.61	4.67
1447	↓	Large	13.88	2.33	3412	96.15	30.91	27.01
1448	↓	↓	13.88	2.22	3780	108.30	35.22	27.31
1446	↓	↓	19.77	0.83	3321	46.22	2.56	4.65
1449	0	Large	19.77	0.81	3463	48.49	2.71	4.69

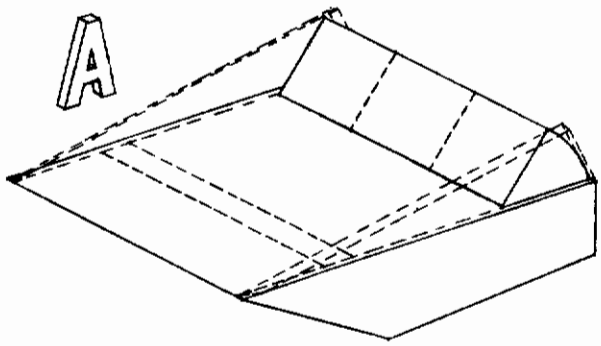

Separated Flows ahead of a Ramp
Fore and aft flaps, end plates
3 separate models:

1) Pressure and heat transfer, AEDC Tunnels A & B, M = 5 & 8, results in Refs. 5-7.

2) Controlled wall temperature, pressure, AEDC Tunnel B, M = 8, results in Refs. 6 and 8.

3) Pressure and heat transfer, Grumman Shock Tunnel, M $\approx$ 13 & 19, results herein.

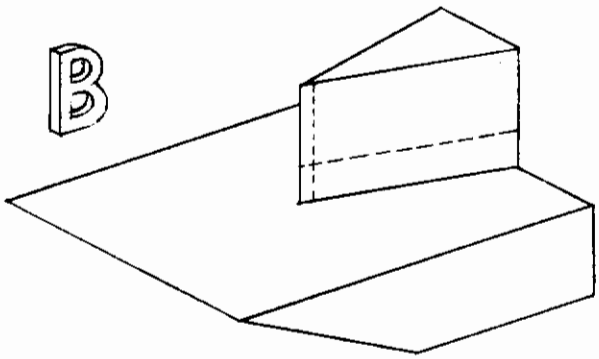

Wedge - Plate Interaction
Small and large fins with sharp and blunt leading edges
2 separate models:

1) Pressure and heat transfer, AEDC Tunnels A & B, M = 5 & 8, results in Refs. 6,7,9 and 10.

2) Pressure and heat transfer, Grumman Shock Tunnel, M $\approx$ 13 & 19, results herein.

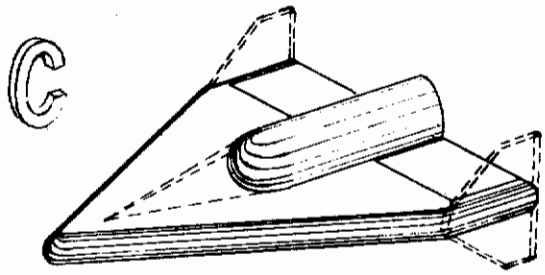

Clipped Delta, Blunt L.E.
Center body, T.E. flaps, drooped nose, spoiler, tip fins
3 separate models:

1) Pressure and heat transfer, AEDC Tunnels A & B, M = 5 & 8, results in Refs. 7 and 11-14.

2) Pressure, AEDC Hotshop 2, M $\approx$ 19, results in Refs. 2 and 15.

3) Six component force, AEDC Tunnels A & B, M = 5 & 8, results in Refs. 14 and 16.

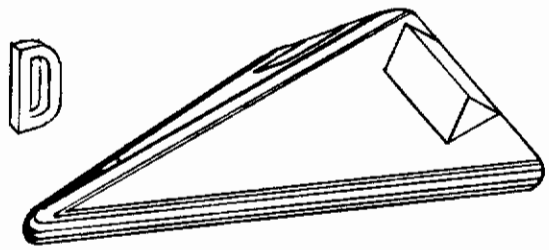

Delta, Blunt L.E., Dihedral
T.E. flaps, canard, ventral fin
3 separate models:

1) Pressure and heat transfer, AEDC Tunnels A & B, M = 5 & 8, results in Refs. 7 and 17-19.

2) Pressure and heat transfer, Grumman Shock Tunnel, M $\approx$ 19, results in Ref. 21.

3) Six component force, AEDC Tunnels A & B, M = 5 & 8, results in Refs. 19 and 20.

Fig. 1 General Outline of Models and Remarks for Over-all Program

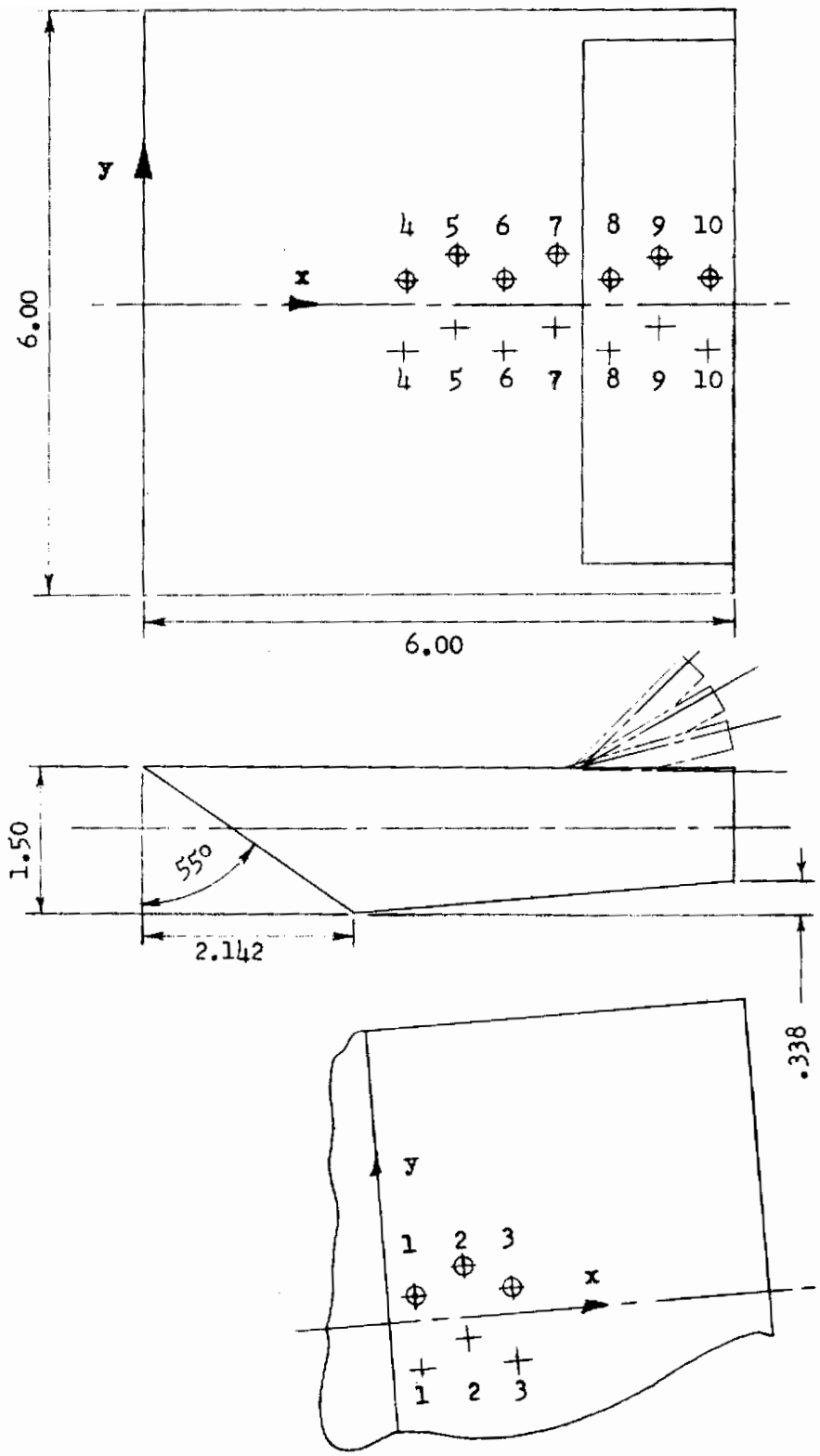

Fig. 2 Dimension and Instrumentation Location for Model A

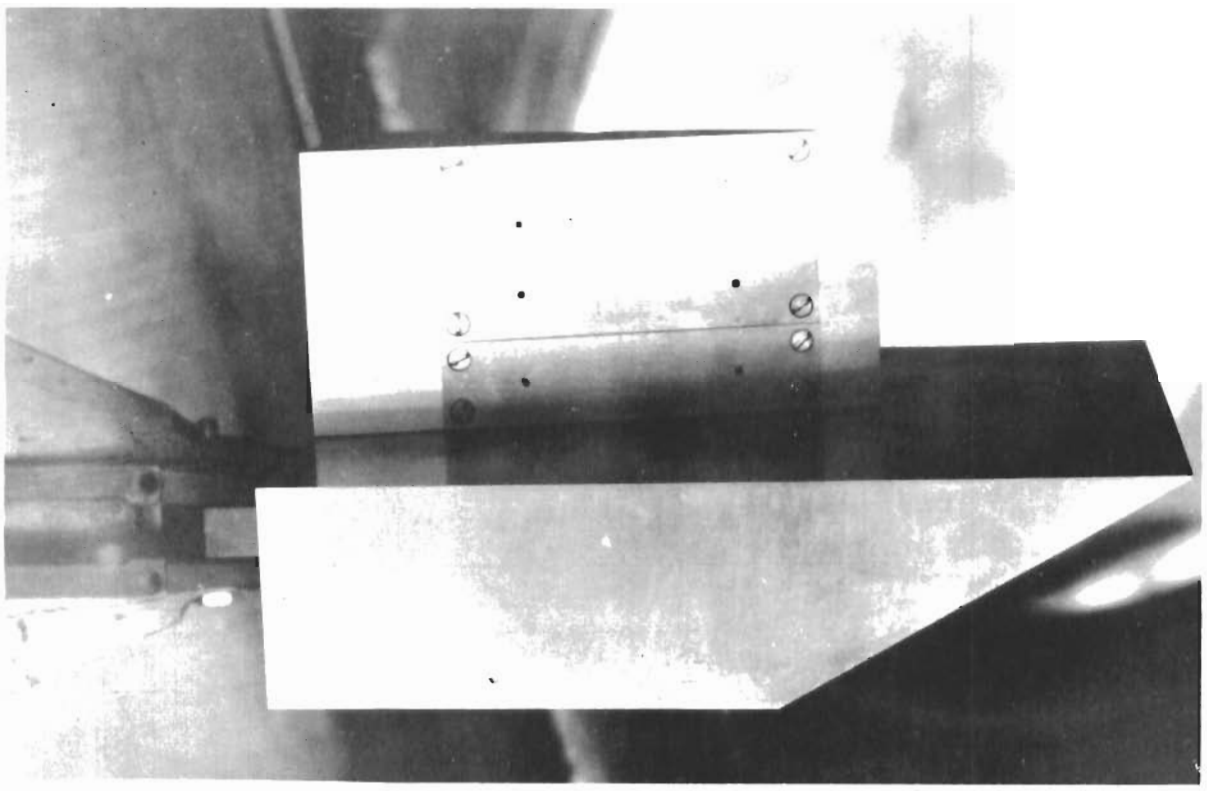

Fig. 3 Photograph Showing Model B with the 2 in. Wedge-Fin

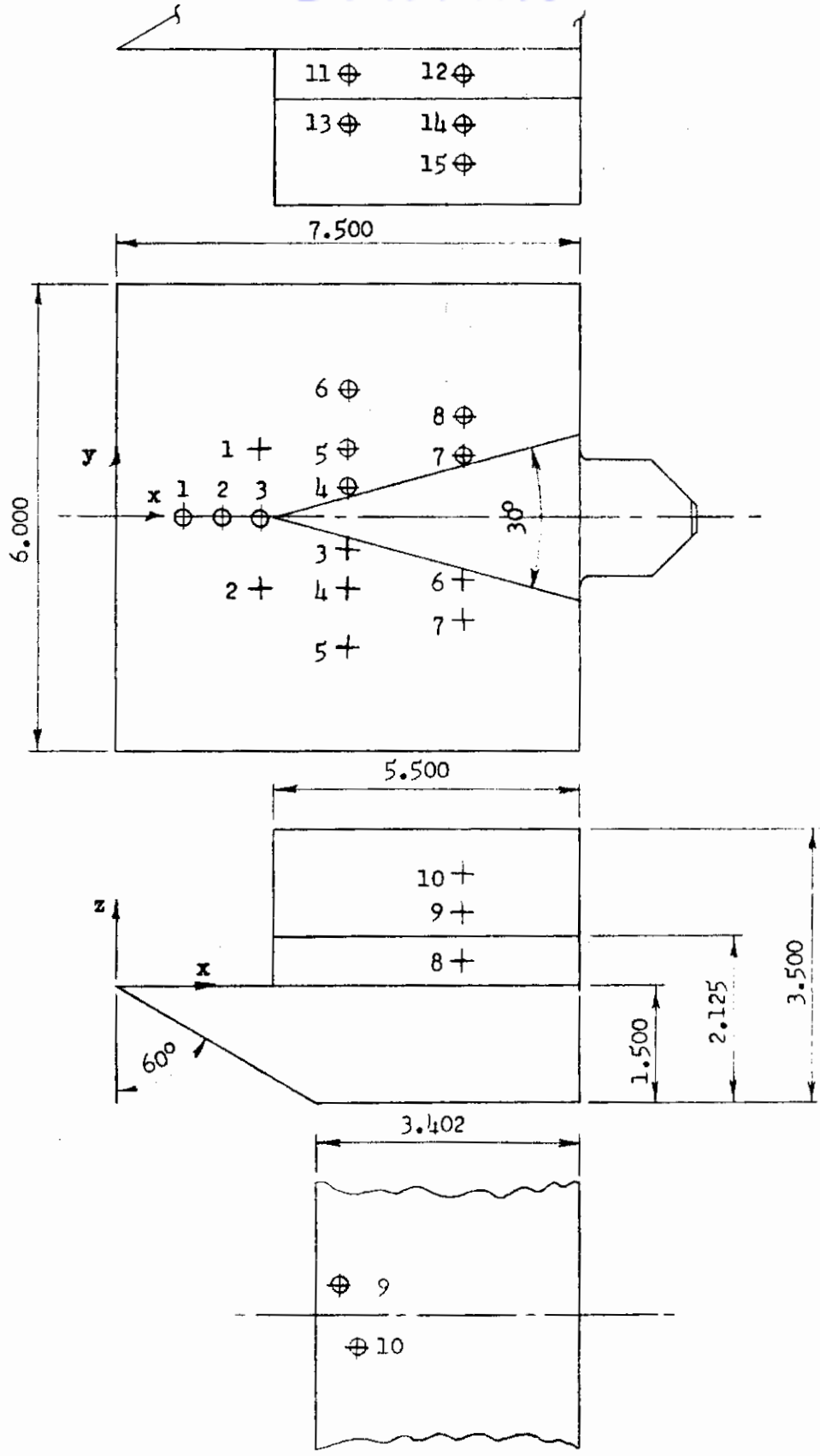

Fig. 4 Dimensions and Instrumentation for Model B

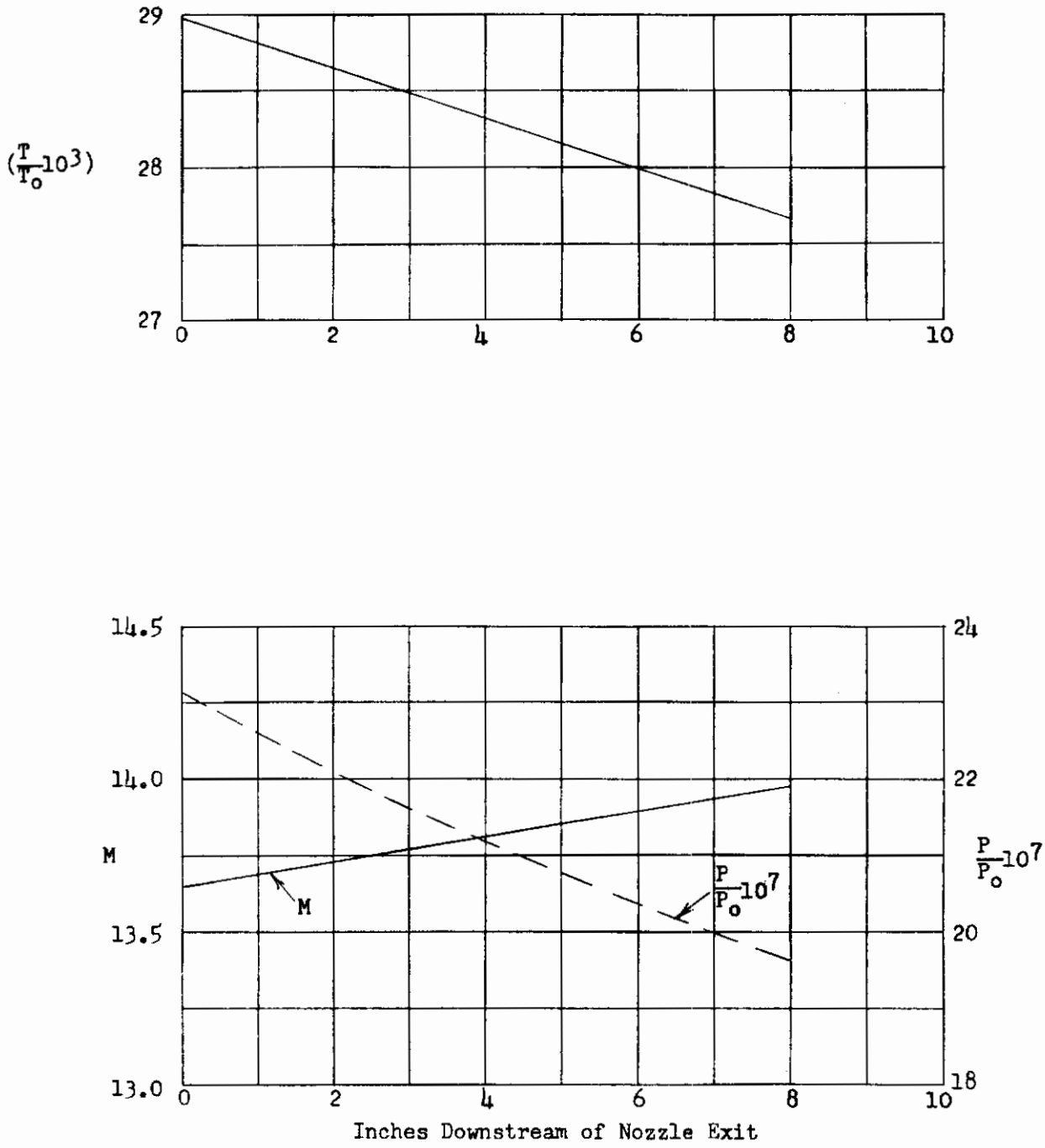

Fig. 5 Tunnel Centerline Distributions of Mach Number and Static to Total Pressure and Temperature Ratios for the M=13 Conditions

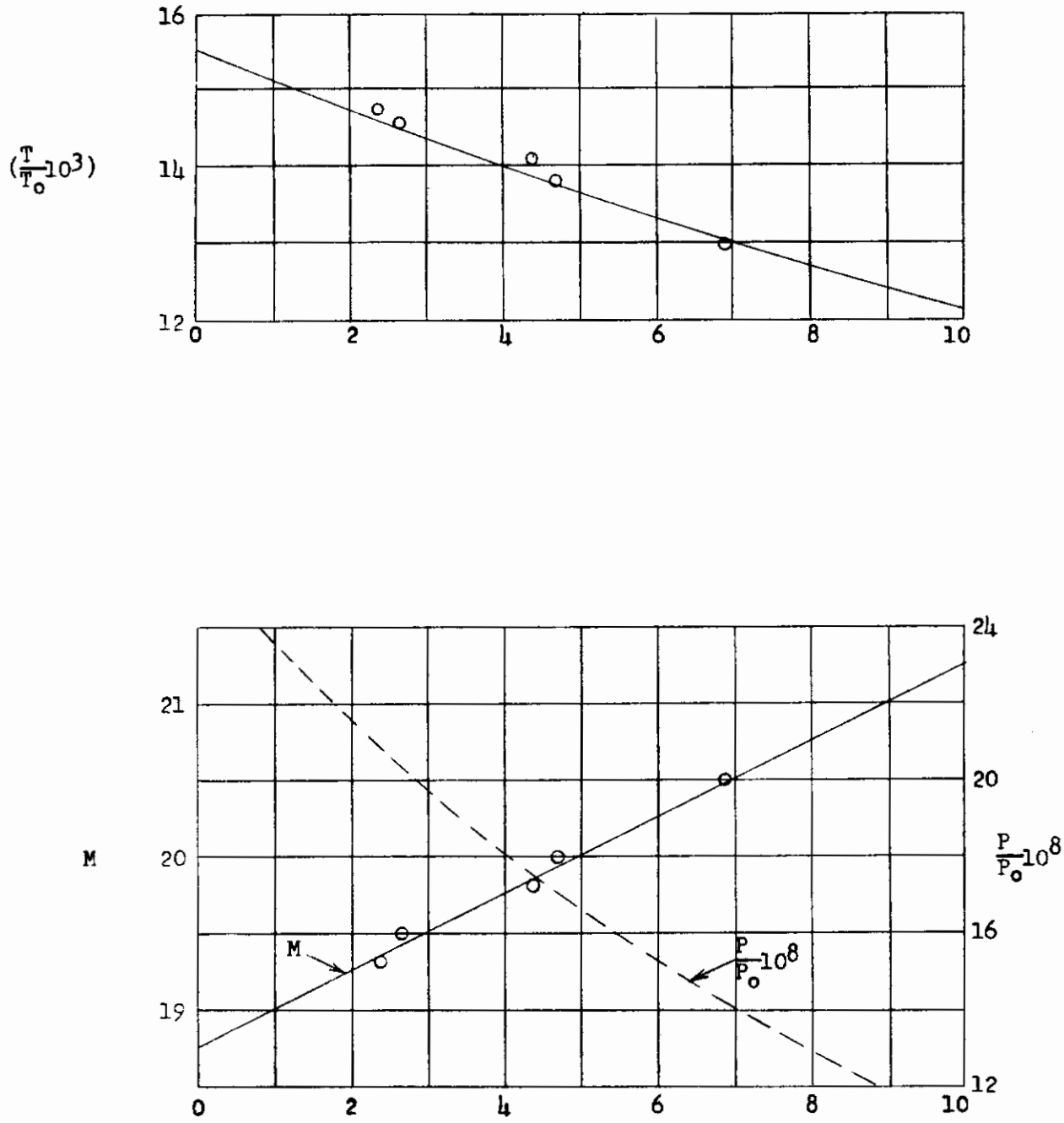

Fig. 6 Tunnel Centerline Distributions of Mach Number and Static to Total Pressure and Temperature Ratios for the M=19 Conditions

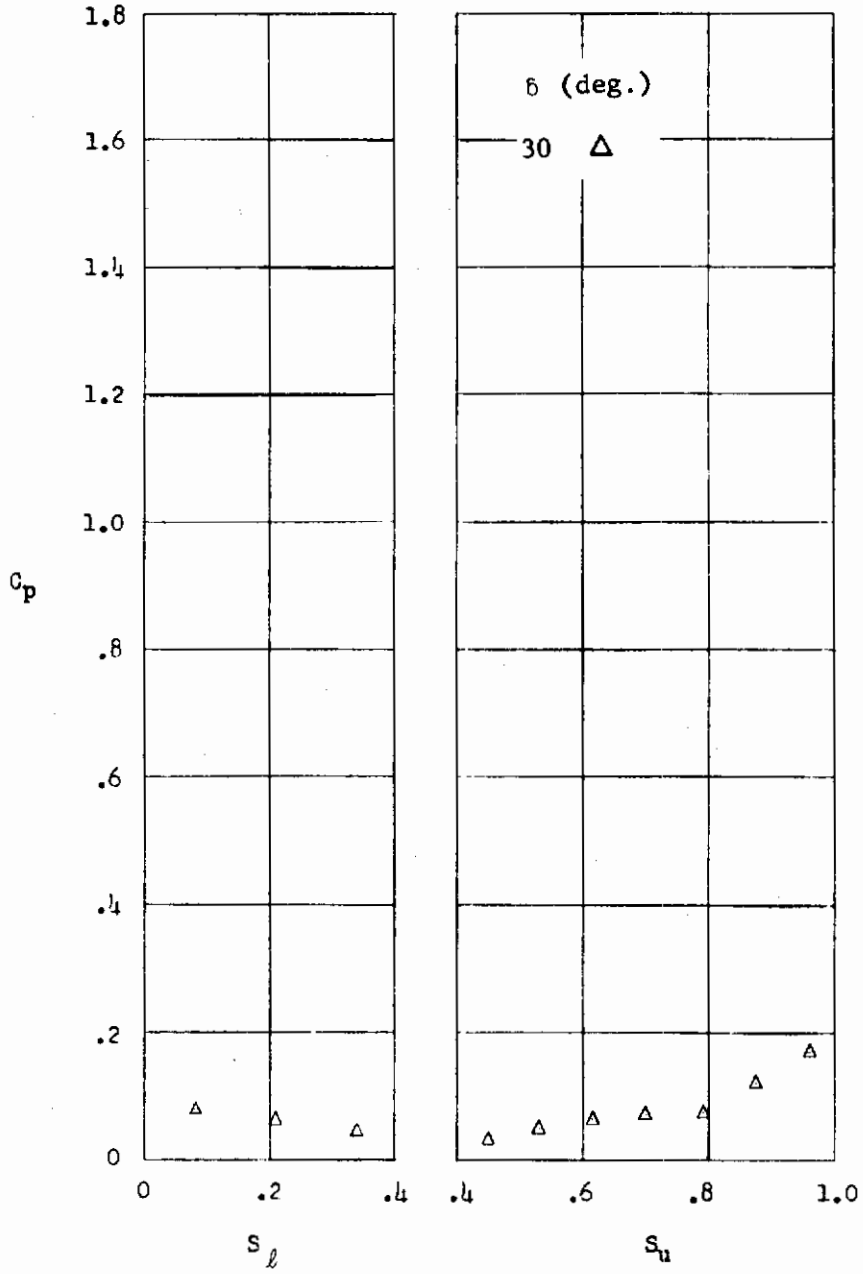

Fig. 7 Chordwise Pressure Distribution for Model A, $M_\infty = 13$, $\alpha = 0$

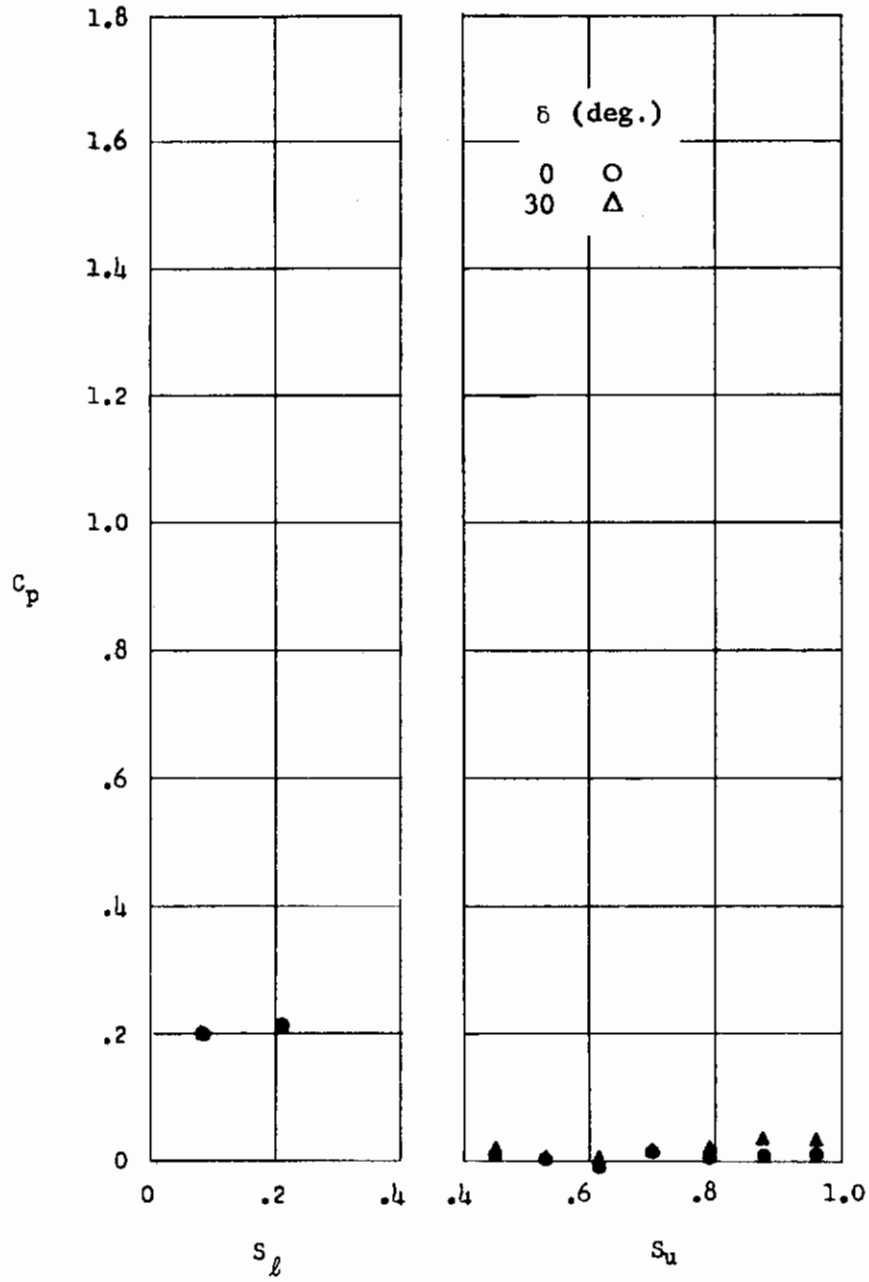

Fig. 8 Chordwise Pressure Distribution for Model A, $M_\infty = 13$, $\alpha = -15$

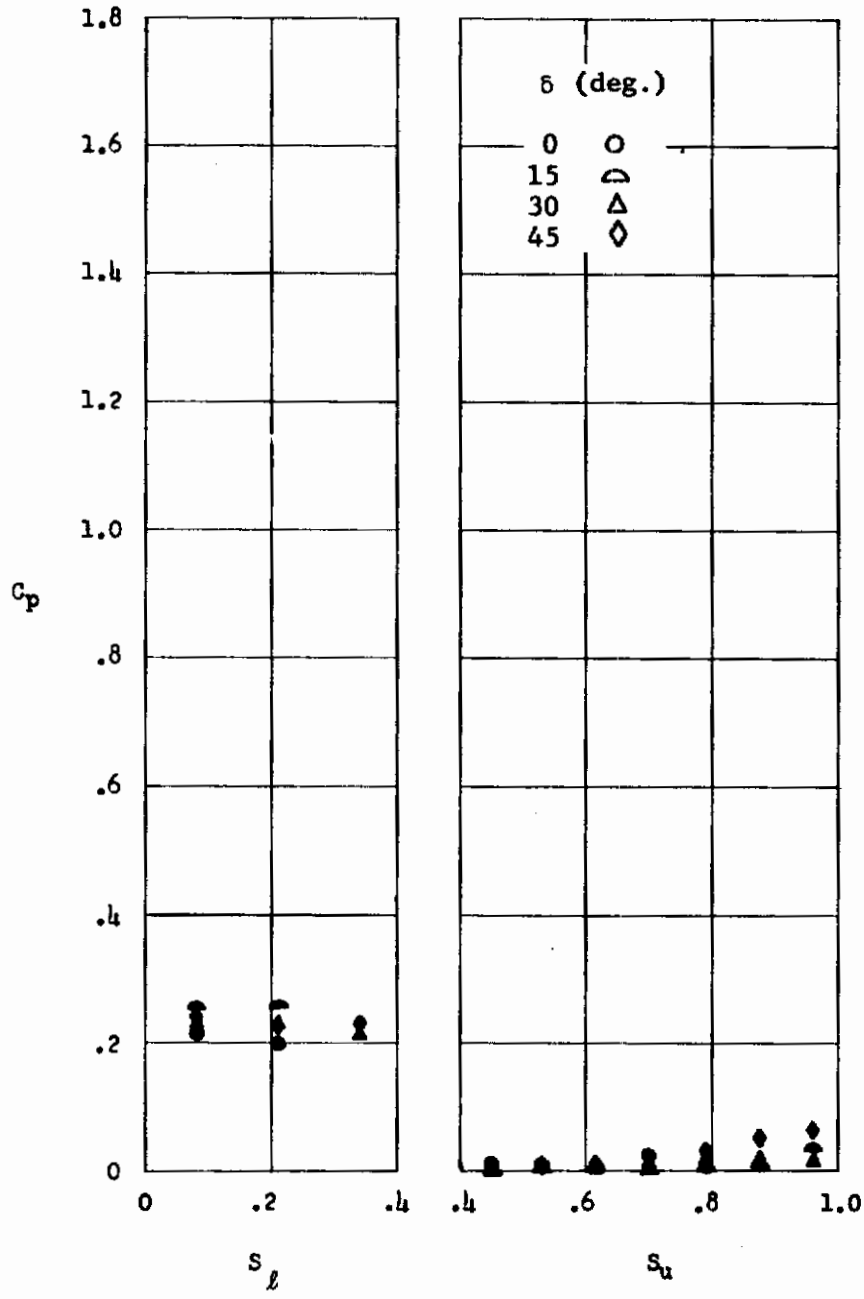

Fig. 9 Chordwise Pressure Distribution for Model A, $M_\infty = 19$, $\alpha = -15$

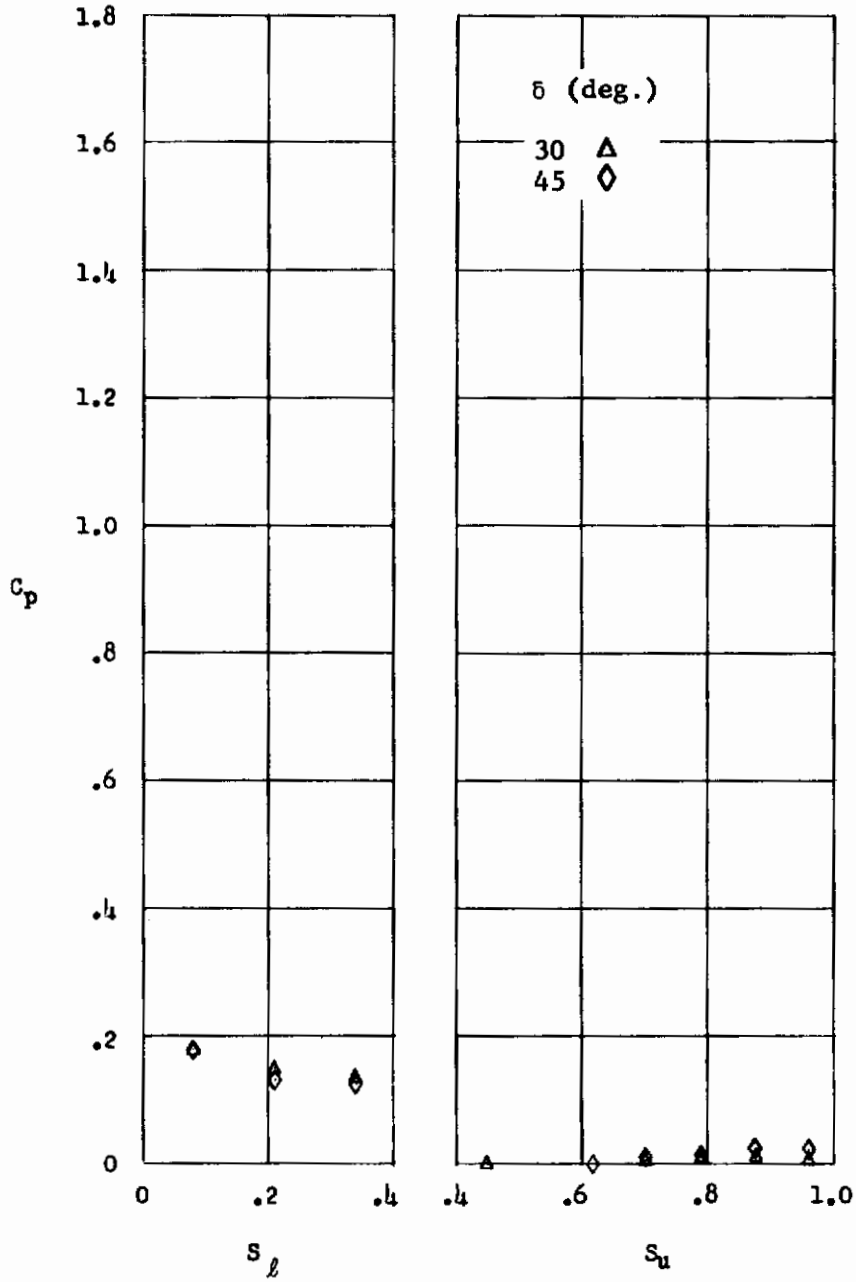

Fig. 10 Chordwise Pressure Distribution for Model A, M_∞ = 19, α = -10

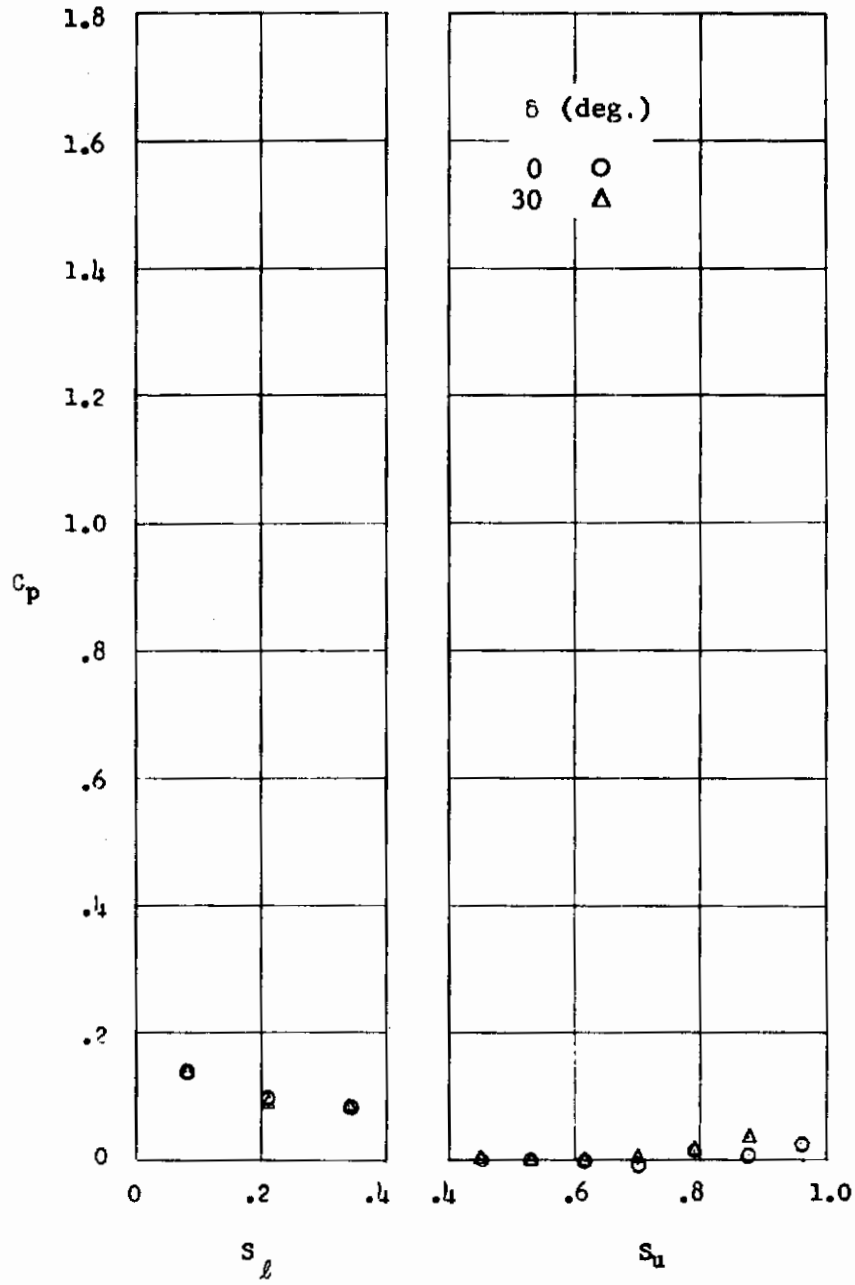

Fig. 11 Chordwise Pressure Distribution for Model A, $M_\infty = 19$, $\alpha = -5$

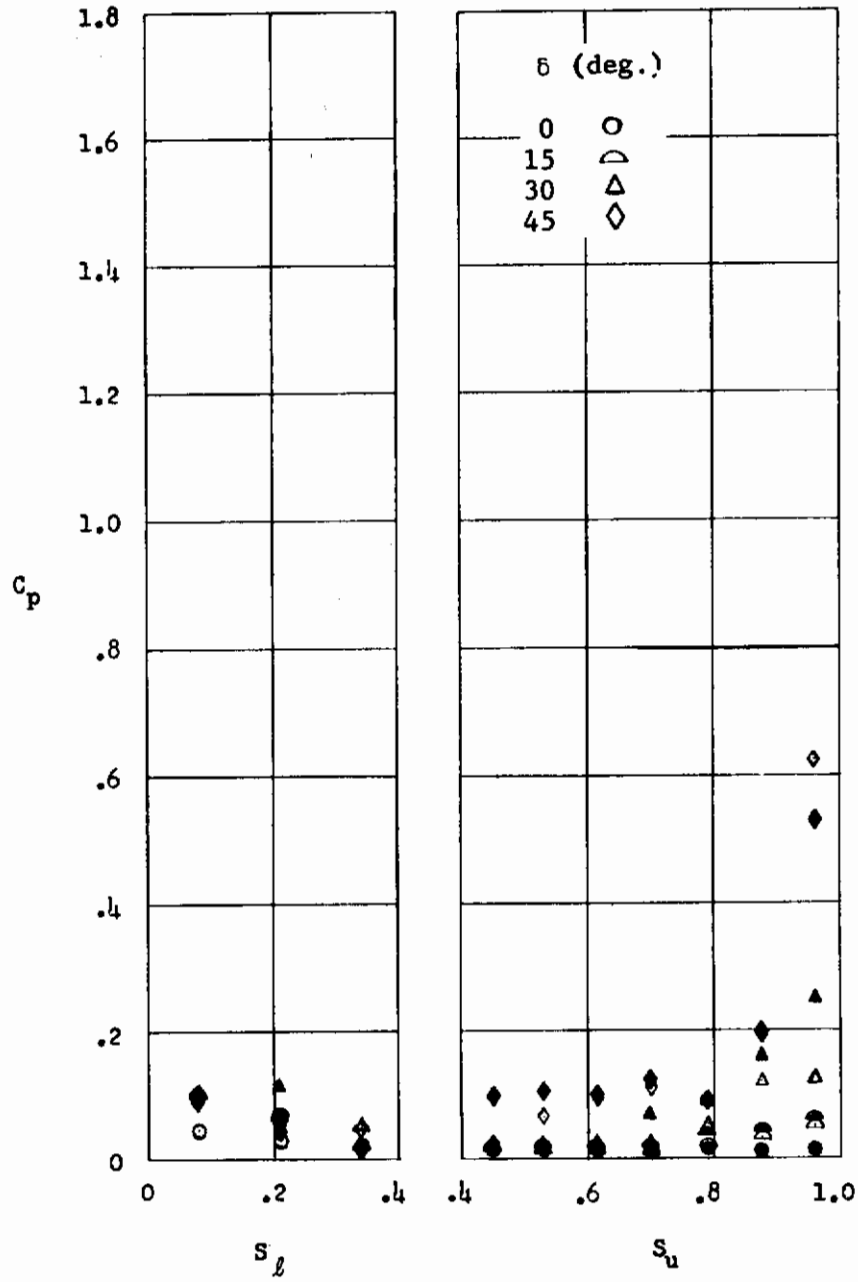

Fig. 12 Chordwise Pressure Distribution for Model A, $M_\infty = 19$, $\alpha = 0$

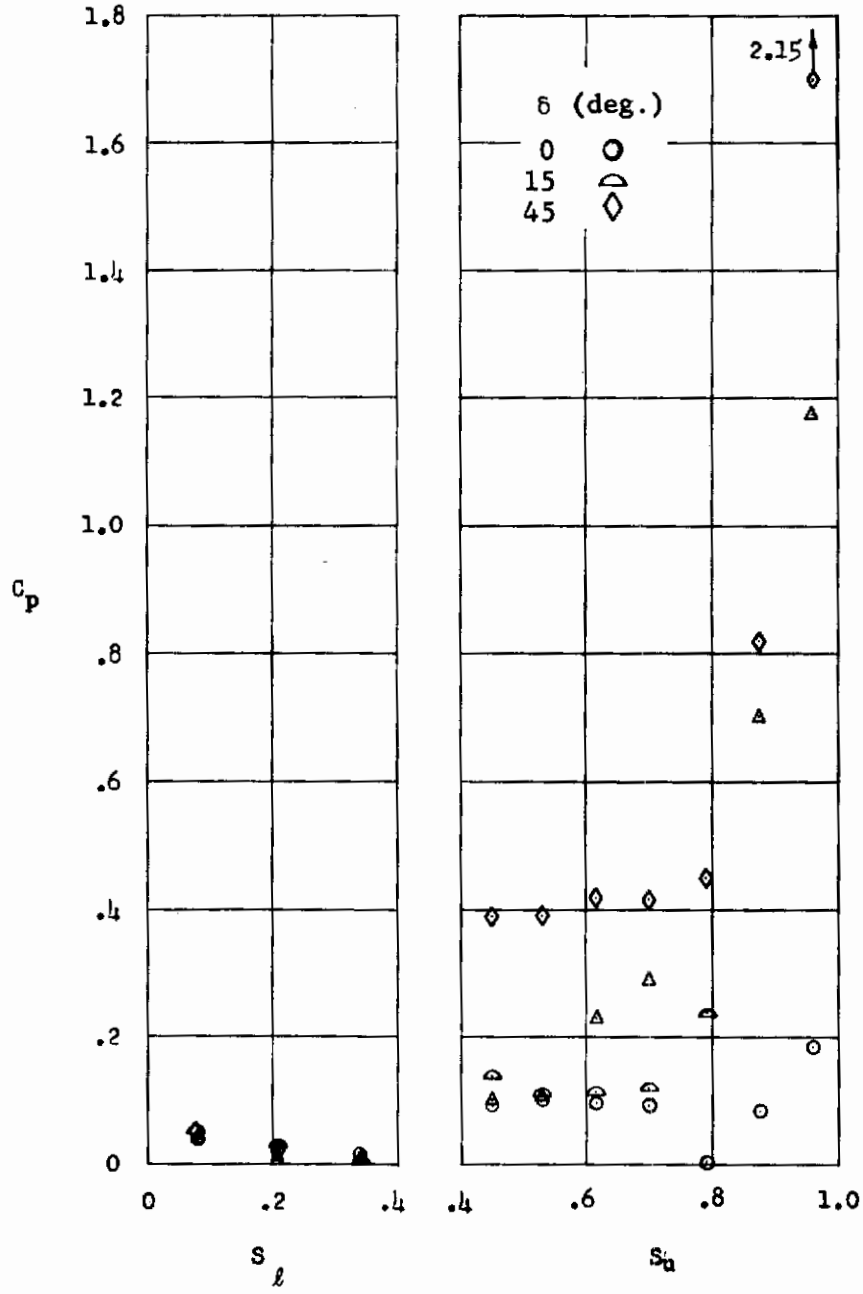

Fig. 13 Chordwise Pressure Distribution for Model A, $M_\infty = 19$, $\alpha = 10$

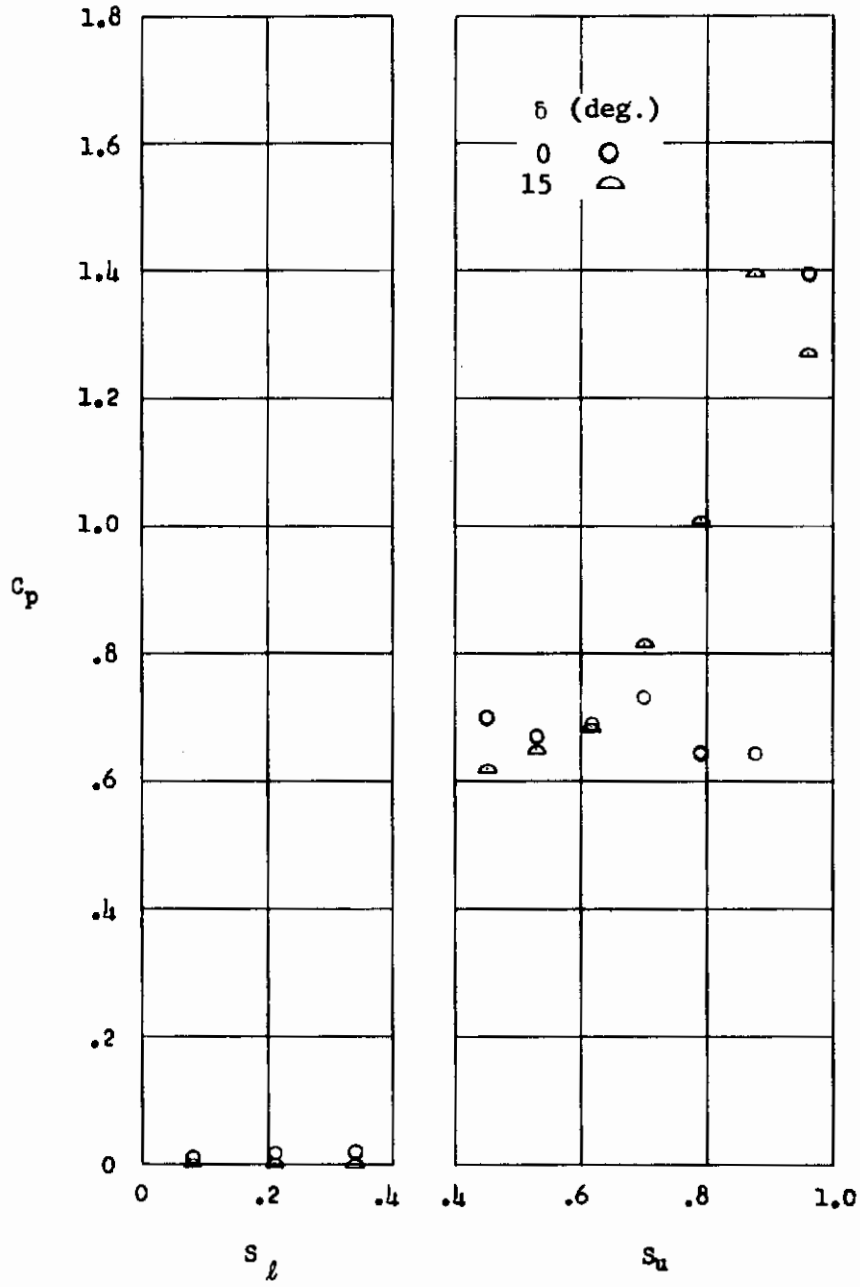

Fig. 14 Chordwise Pressure Distribution for Model A, M_∞ = 19, α = 30

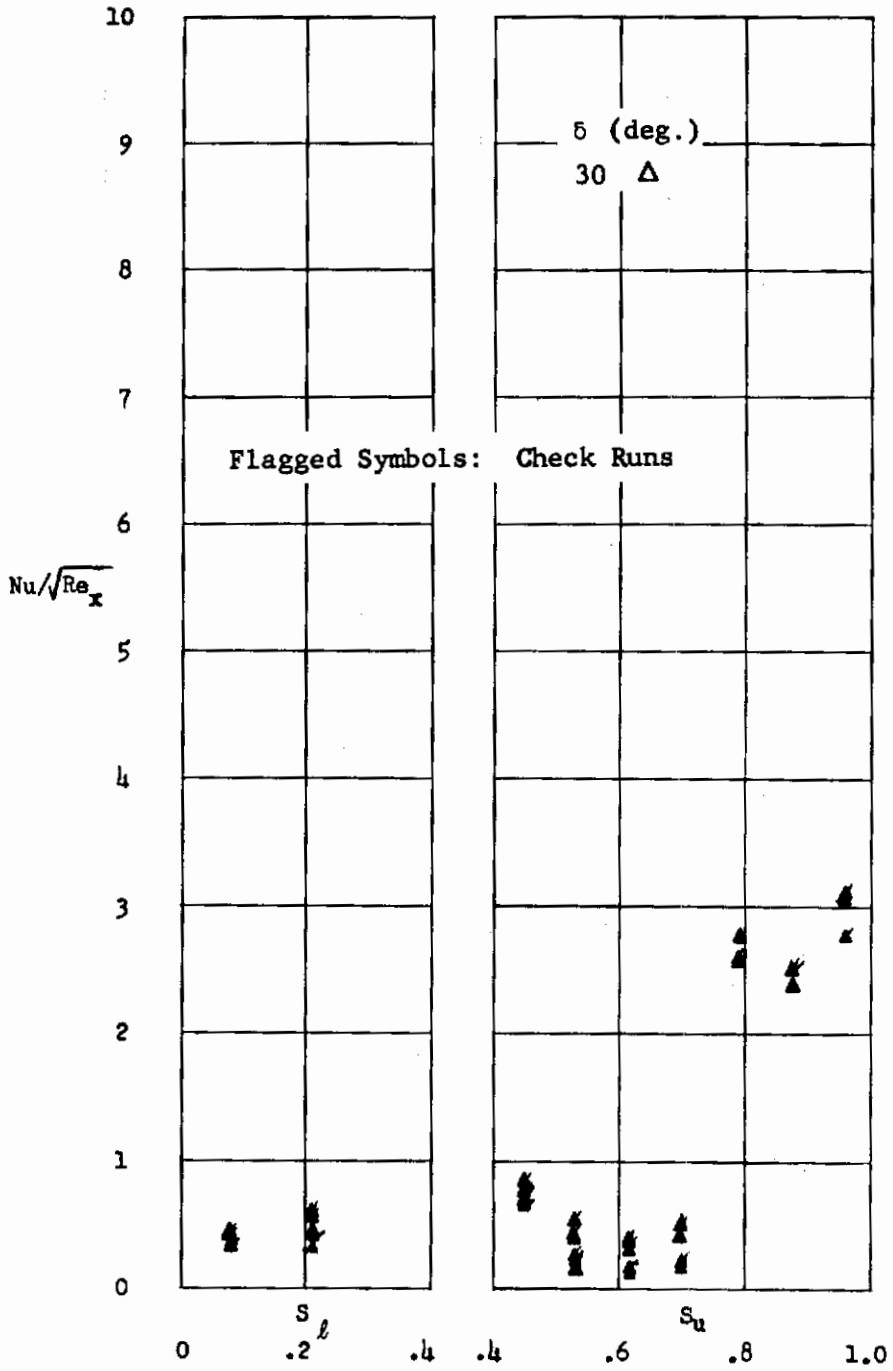

Fig. 15 Chordwise Heat Transfer Distribution for Model A, $M_\infty = 13$, $\alpha = 0$

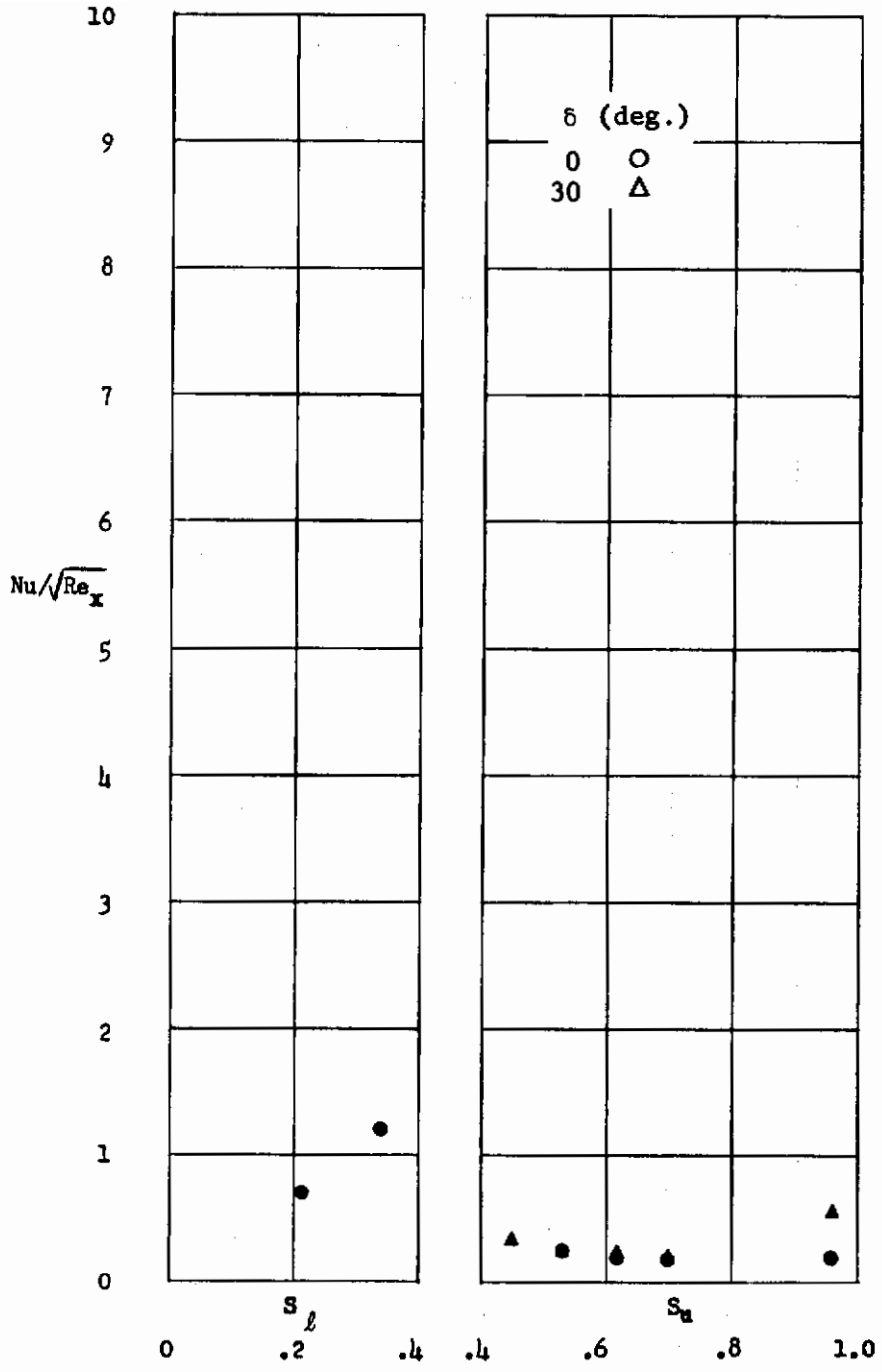

Fig. 16 Chordwise Heat Transfer Distribution for Model A, M_∞ = 13, α = -15

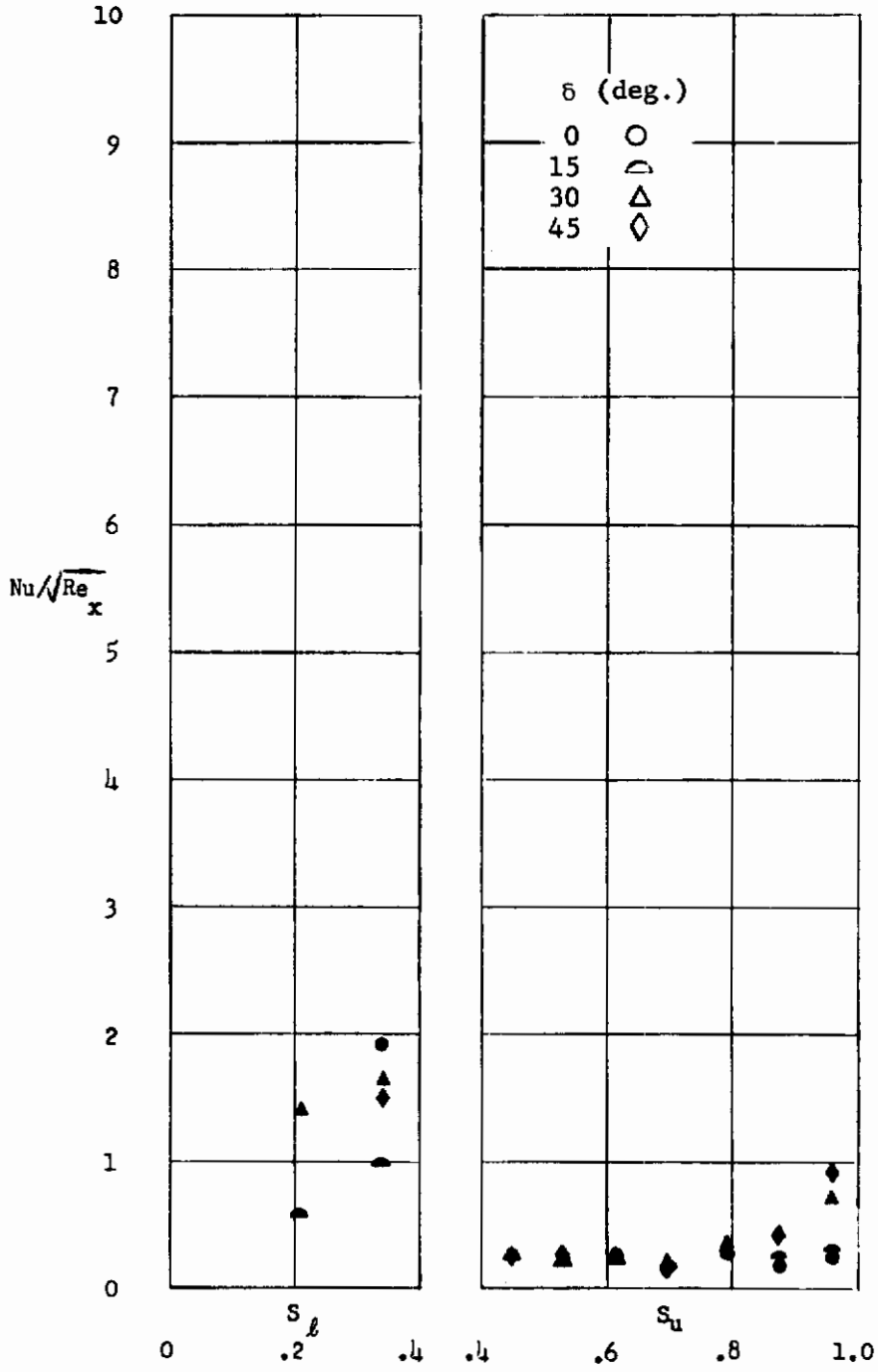

Fig. 17 Chordwise Heat Transfer Distribution for Model A, M_∞ = 19, α = -15

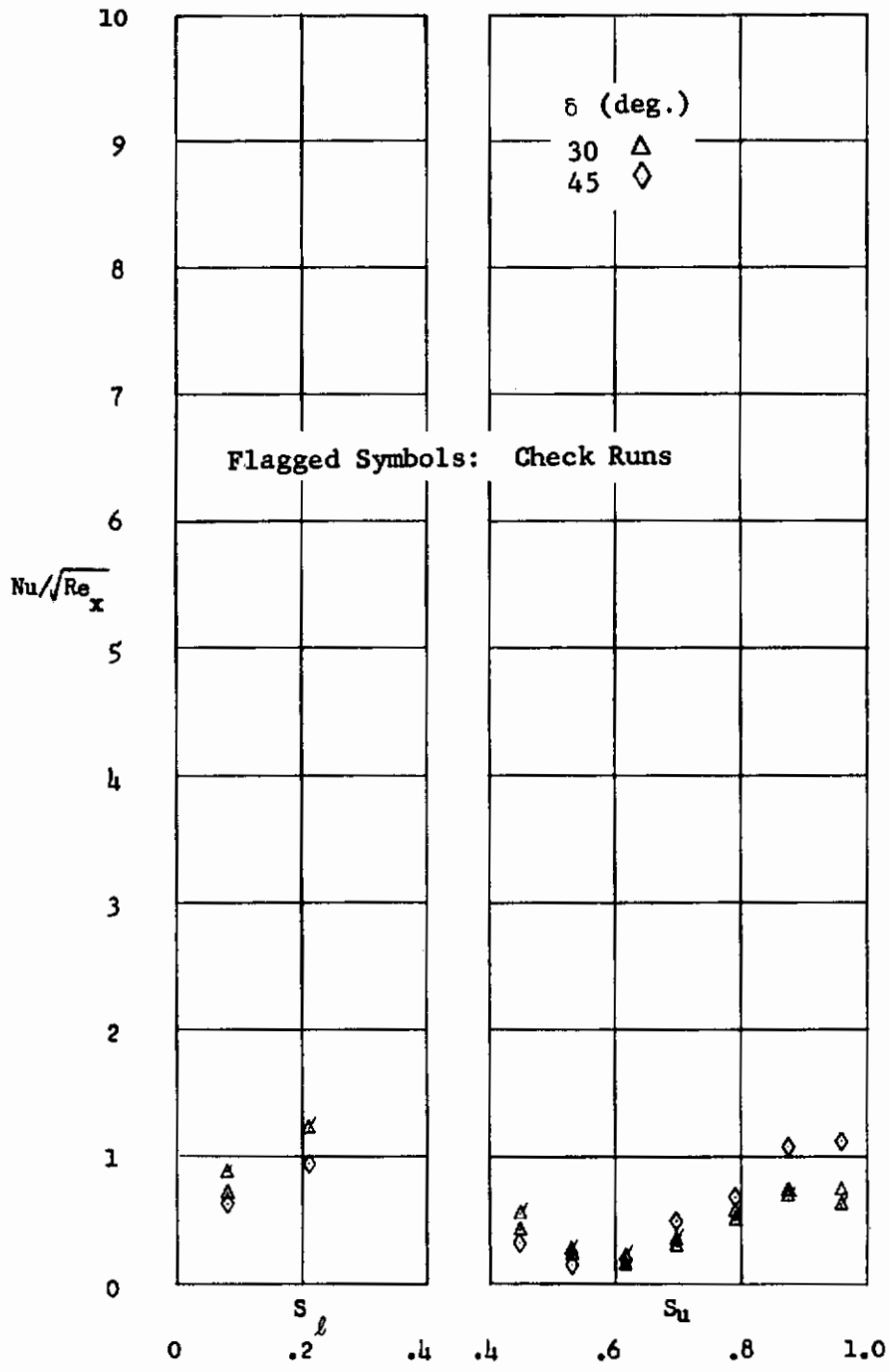

Fig. 18 Chordwise Heat Transfer Distribution for Model A, $M_\infty = 19$, $\alpha = -10$

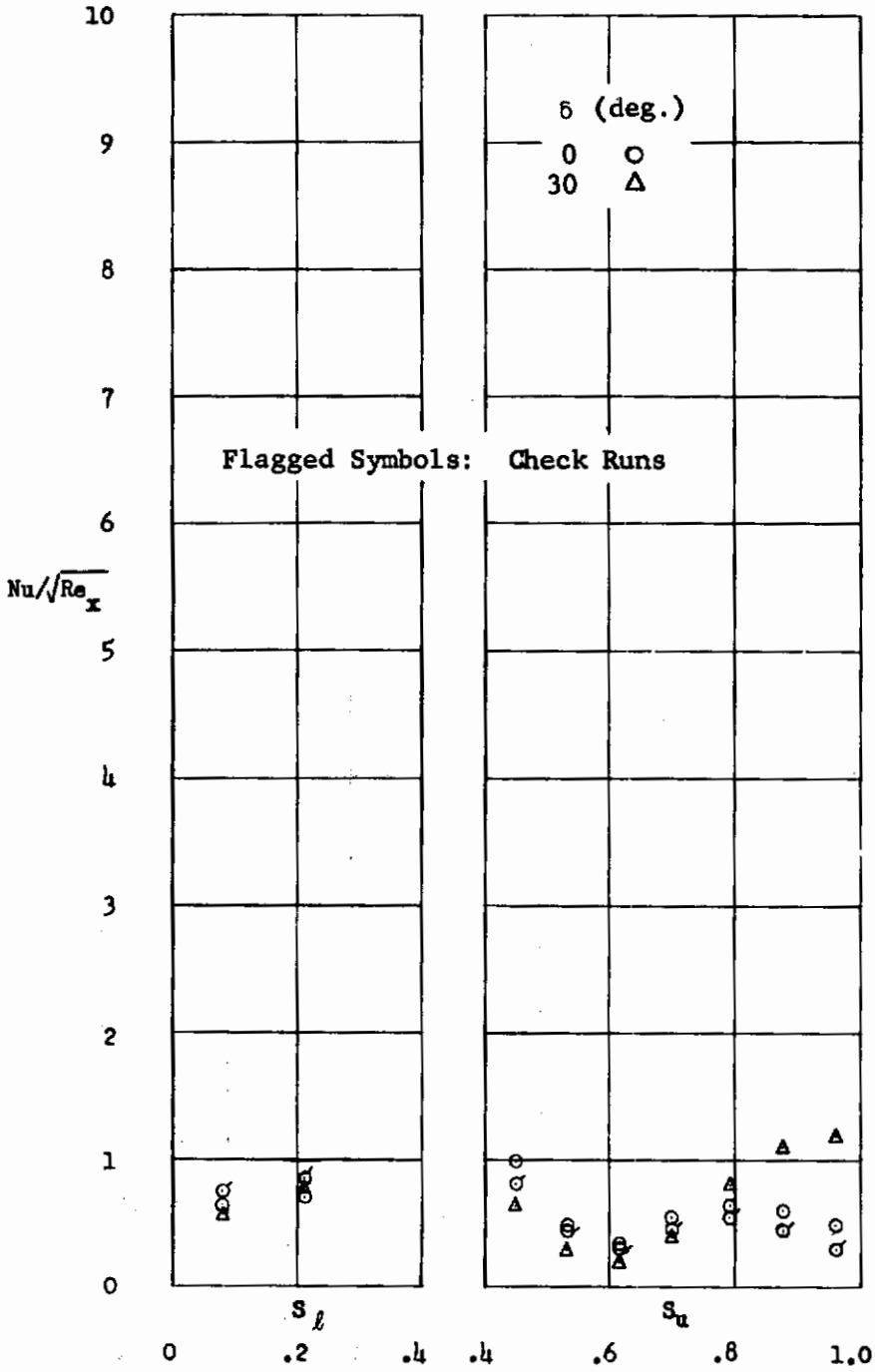

Fig. 19 Chordwise Heat Transfer Distribution for Model A, $M_\infty = 19$, $\alpha = -5$

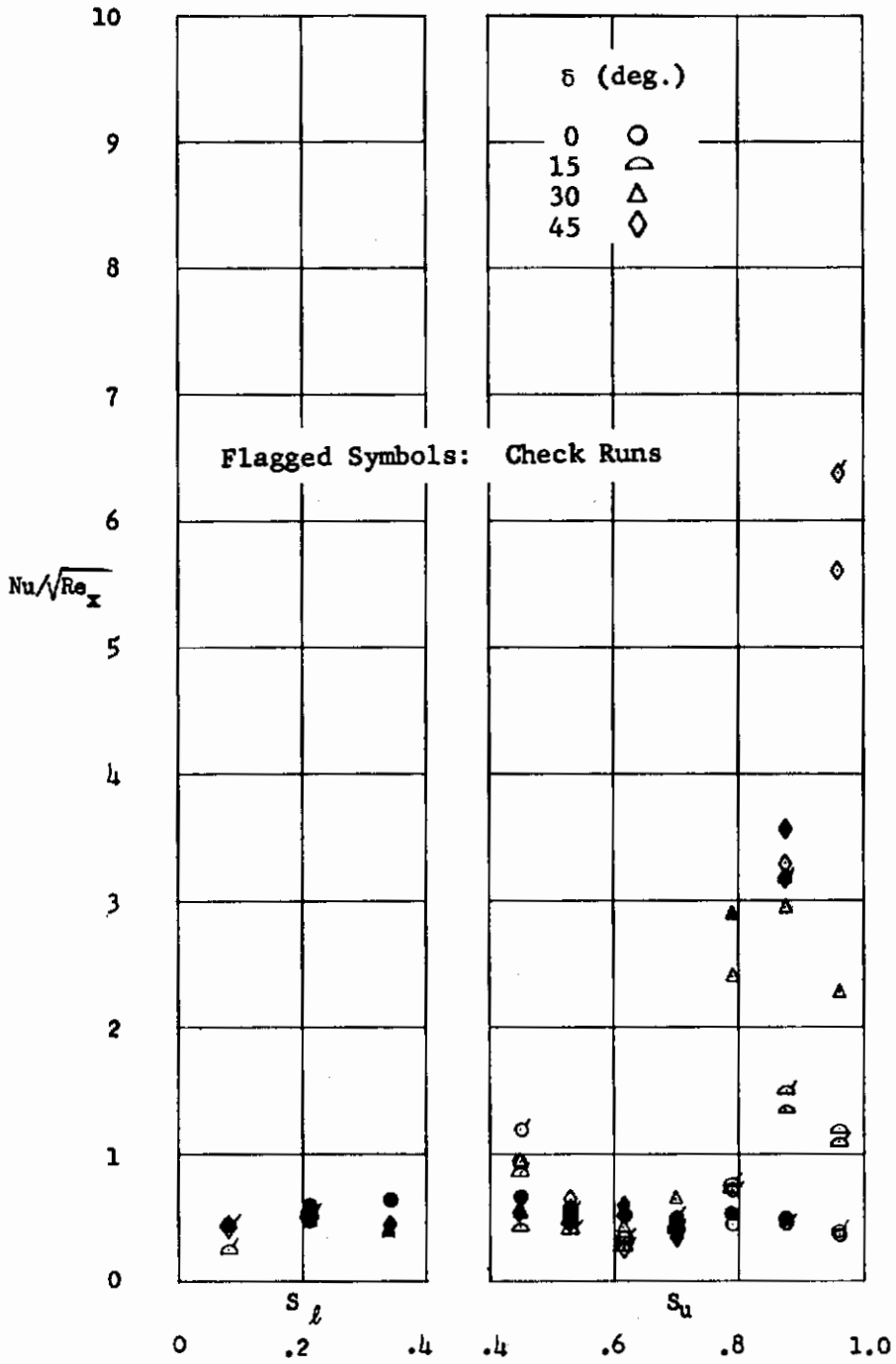

Fig. 20 Chordwise Heat Transfer Distribution for Model A, $M_\infty = 19$, $\alpha = 0$

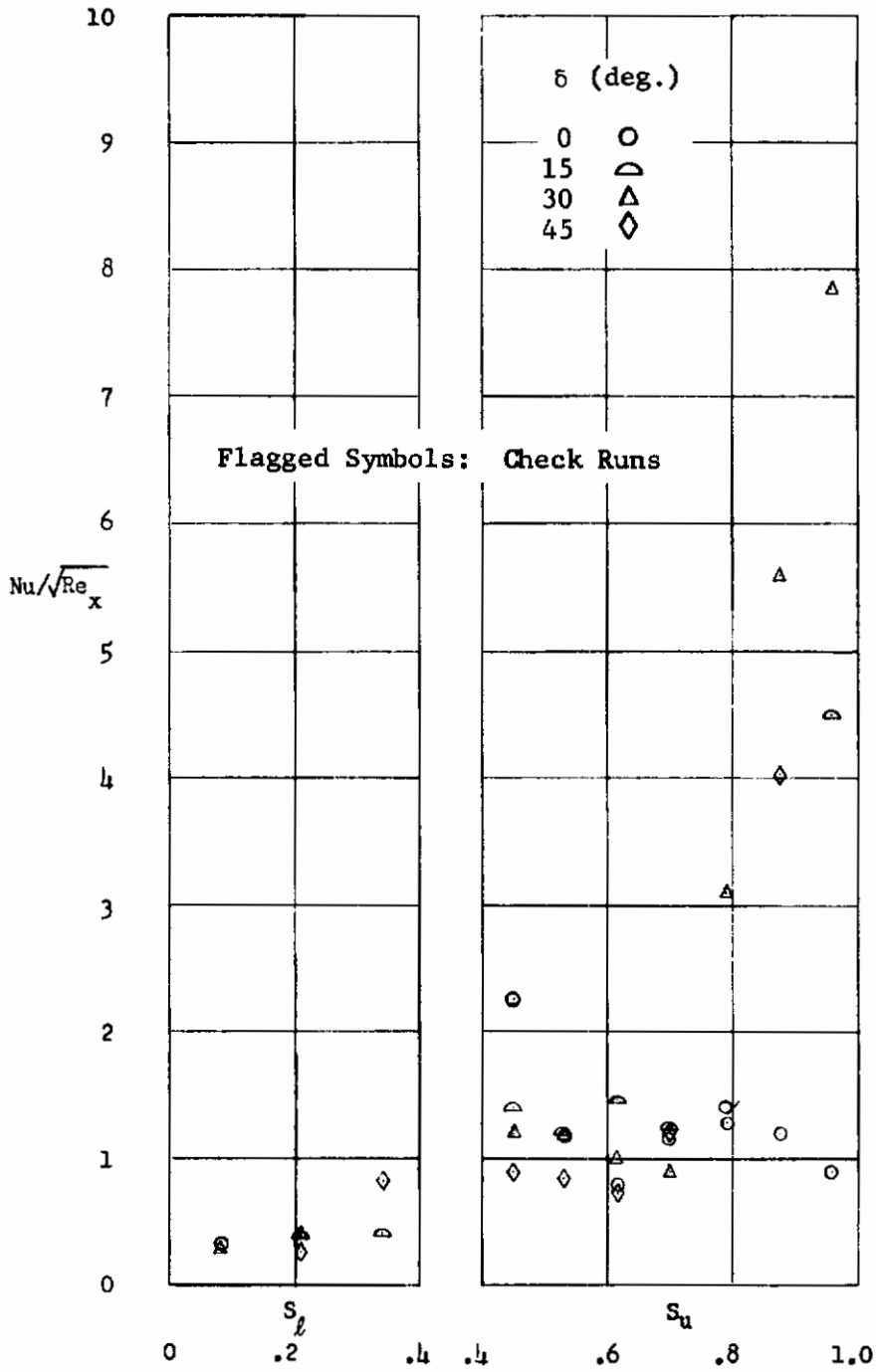

Fig. 21 Chordwise Heat Transfer Distribution for Model A, $M_\infty = 19$, $\alpha = 10$

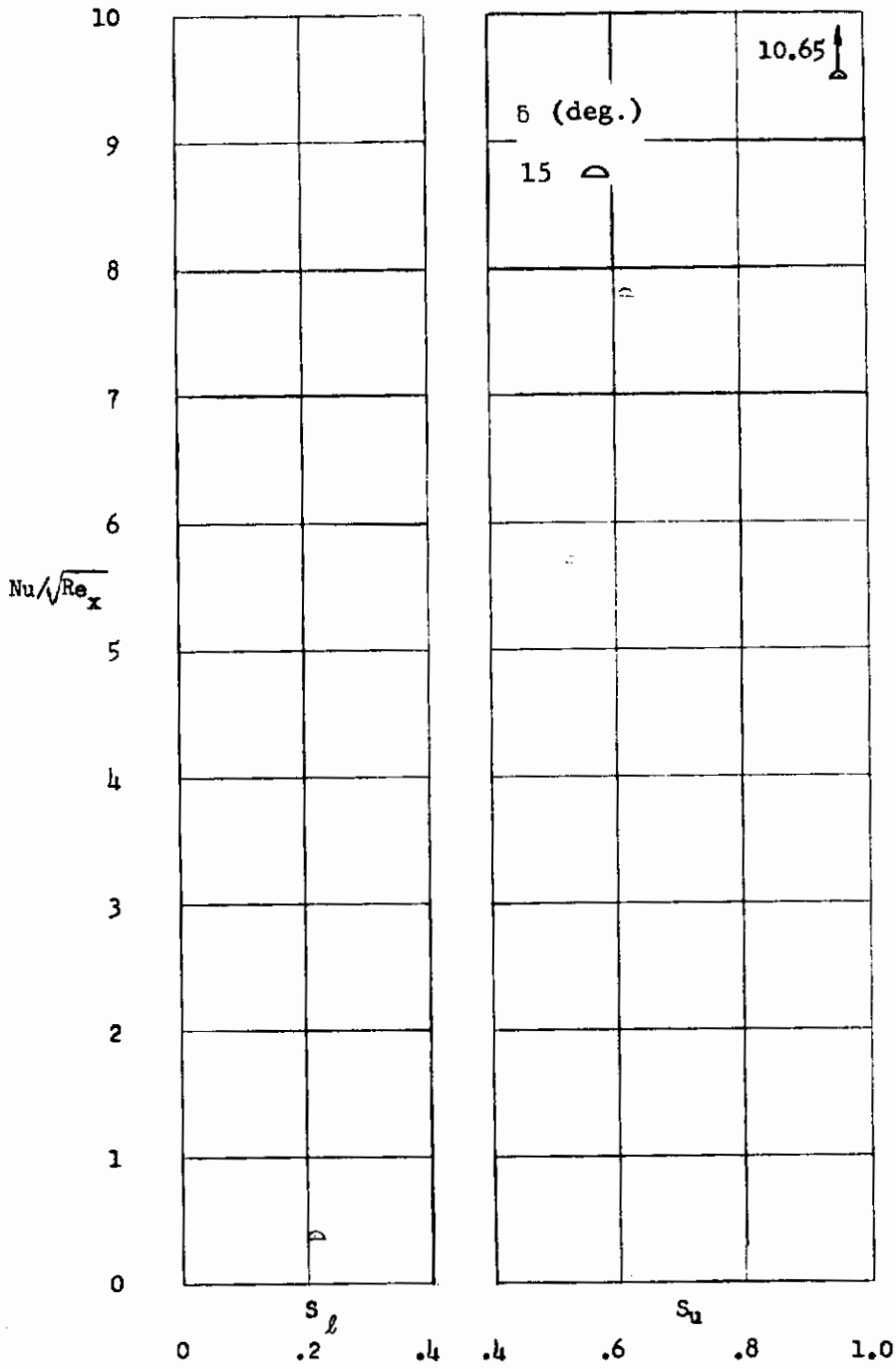

Fig. 22 Chordwise Heat Transfer Distribution for Model A, $M_\infty = 19$, $\alpha = 30$

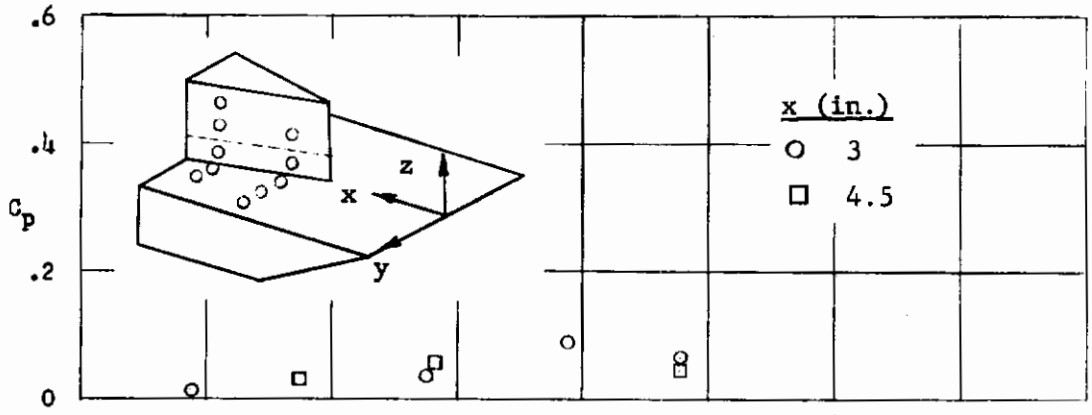

Fig. 23 Wedge Plate Interaction Pressure Data, Small, Sharp LE Wedge, $M_\infty = 19$, $\alpha = 0$

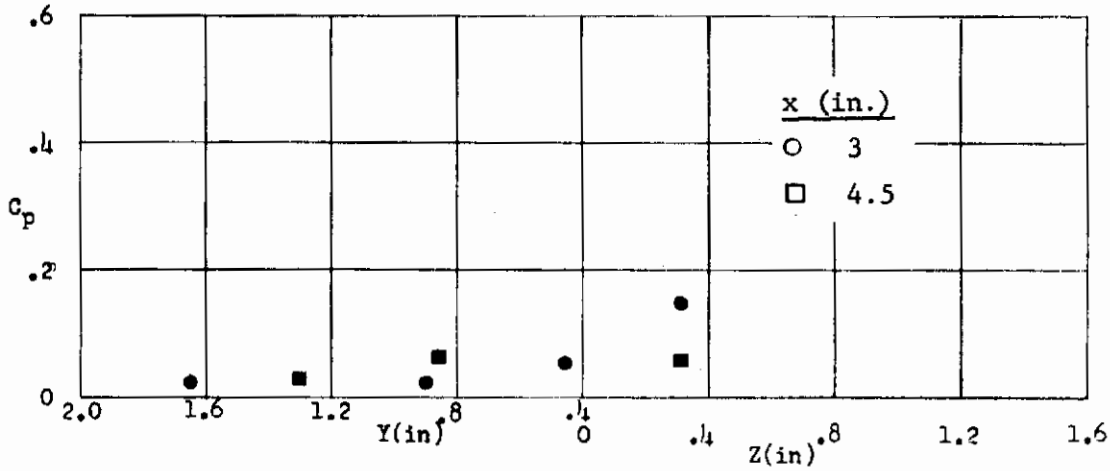

Fig. 24 Wedge Plate Interaction Pressure Data, Small, Sharp LE Wedge, $M_\infty = 13$, $\alpha = 0$

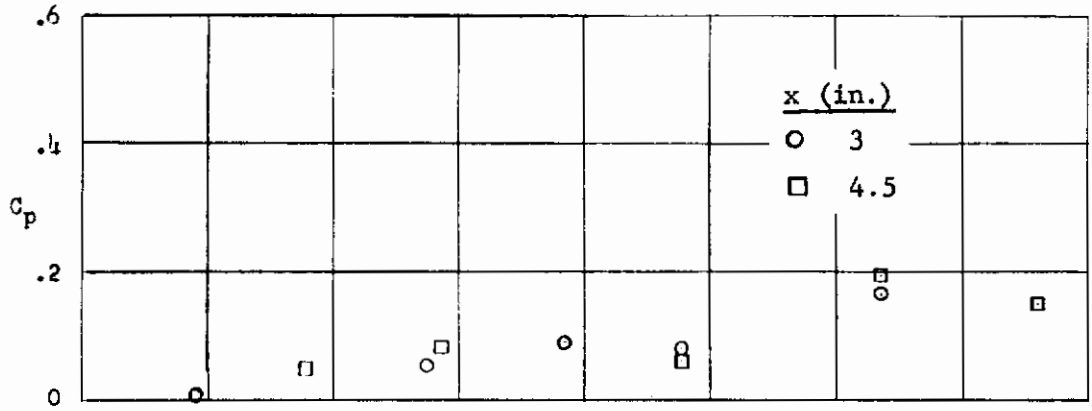

Fig. 25 Wedge Plate Interaction Pressure Data, Large, Sharp LE Wedge, $M_\infty = 19$, $\alpha = 0$

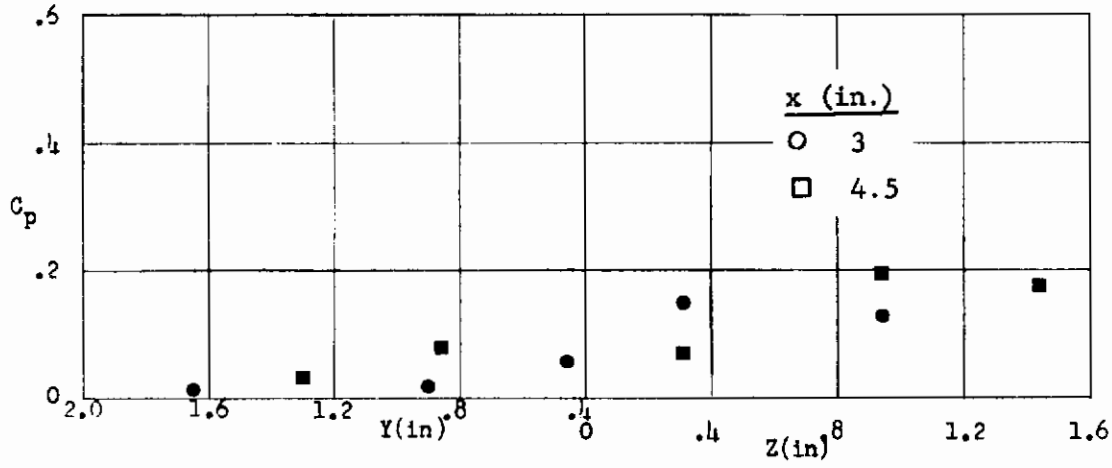

Fig. 26 Wedge Plate Interaction Pressure Data, Large, Sharp LE Wedge, $M_\infty = 13$, $\alpha = 0$

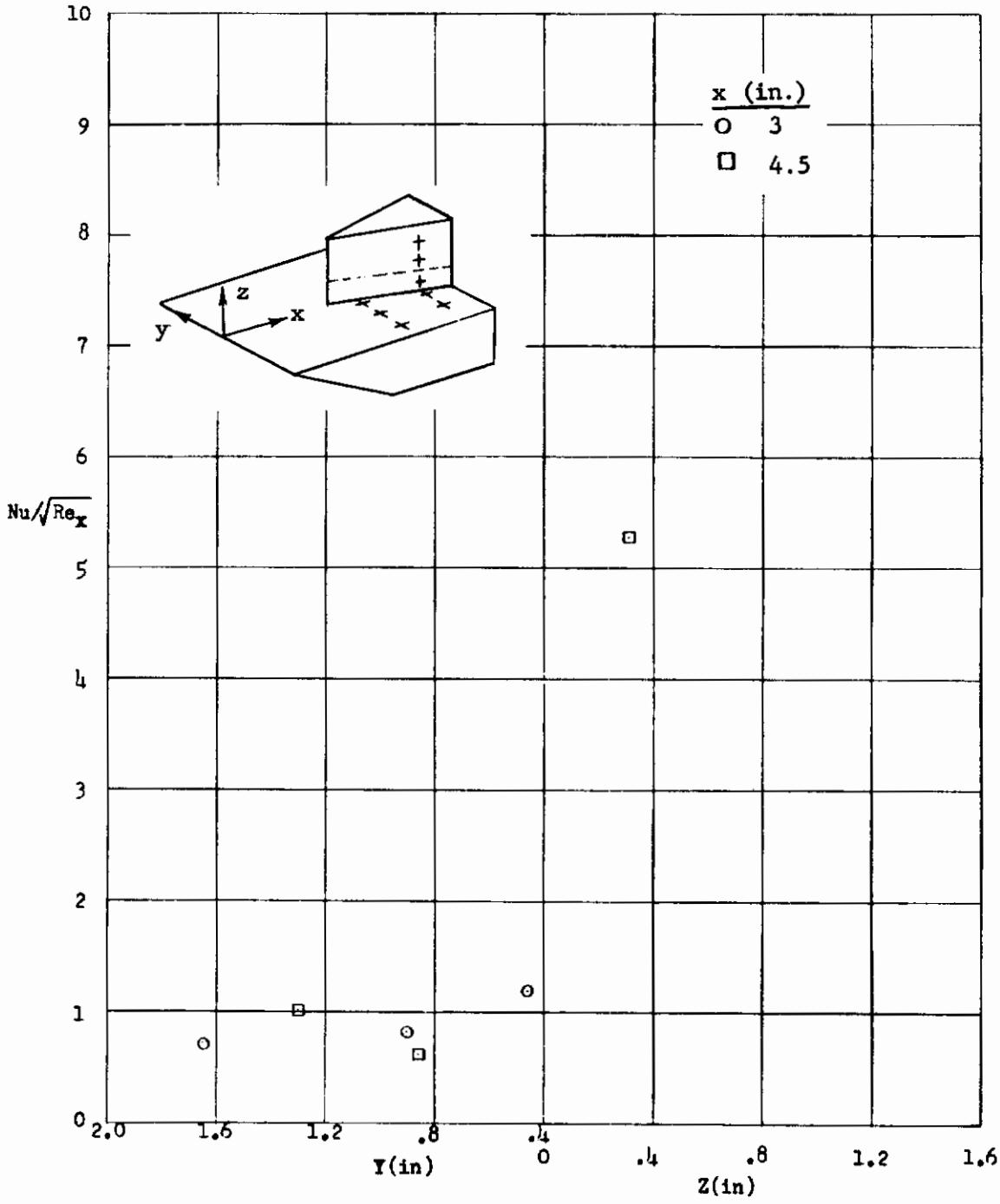

Fig. 27 Wedge Plate Interaction Heat Transfer Data, Small, Sharp LE Wedge, $M_\infty = 19$, $\alpha = 0$

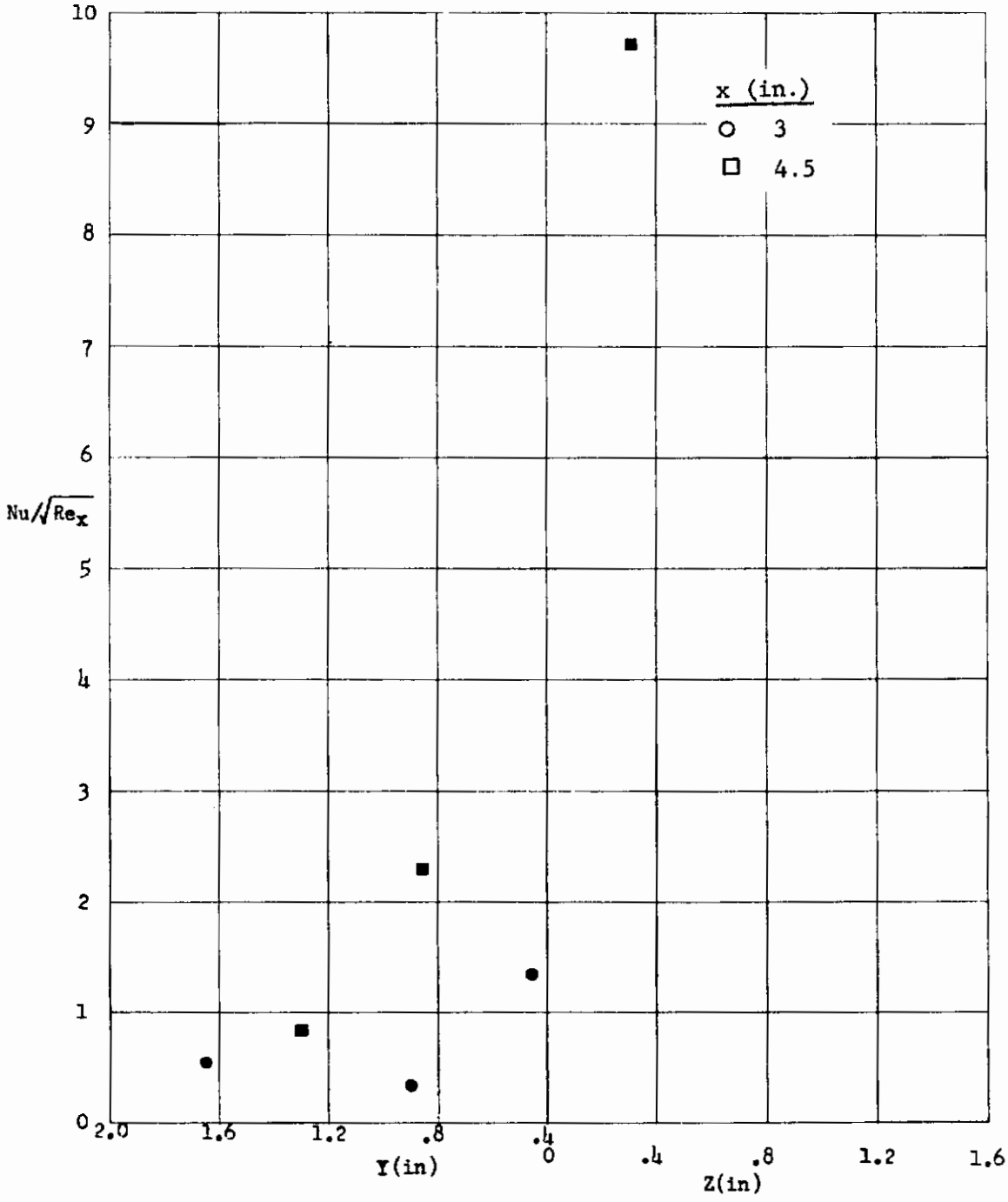

Fig. 28 Wedge Plate Interaction Heat Transfer Data, Small, Sharp LE Wedge, $M_\infty = 13$, $\alpha = 0$

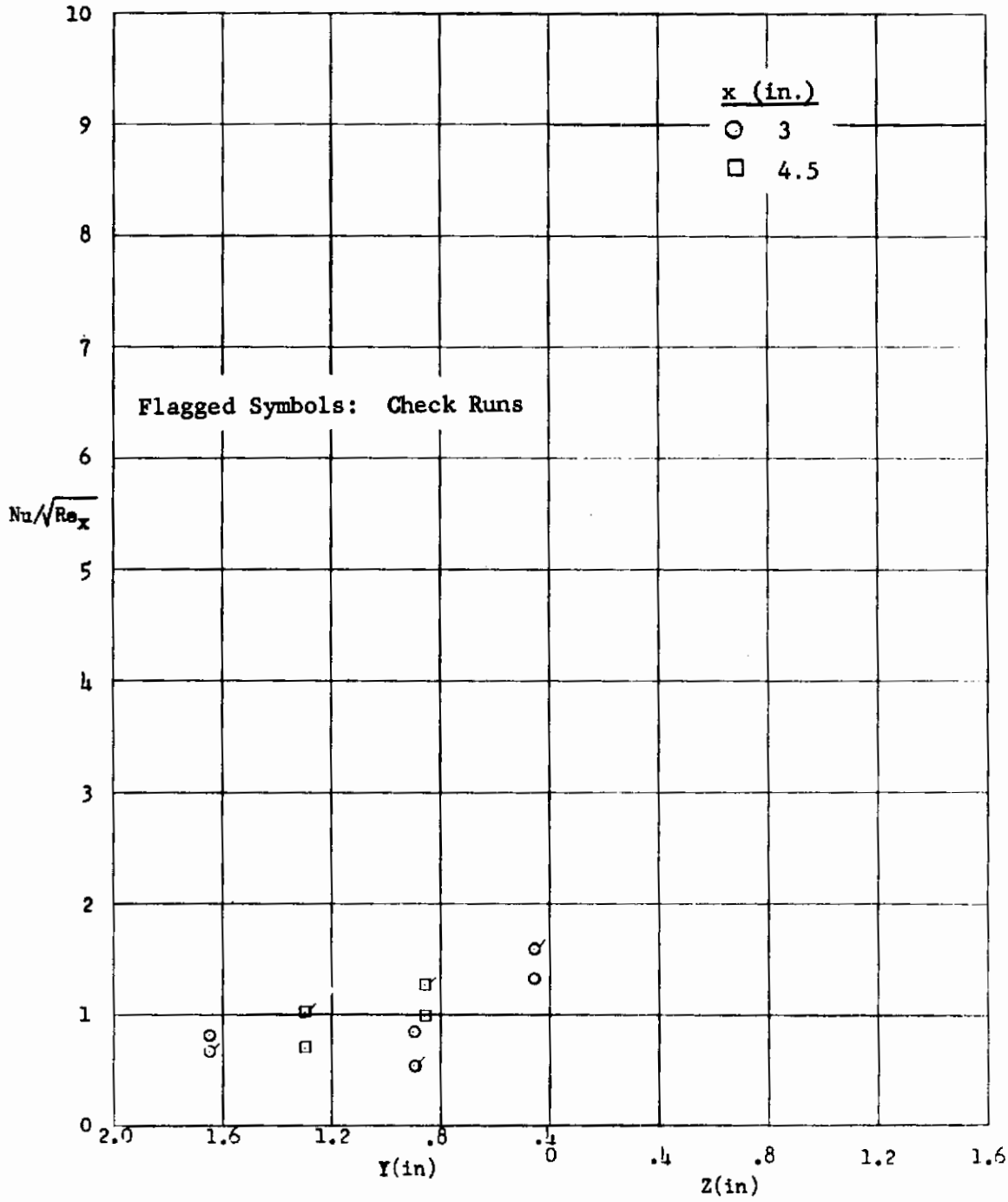

Fig. 29 Wedge Plate Interaction Heat Transfer Data, Large, Sharp LE Wedge, $M_\infty = 19$, $\alpha = 0$

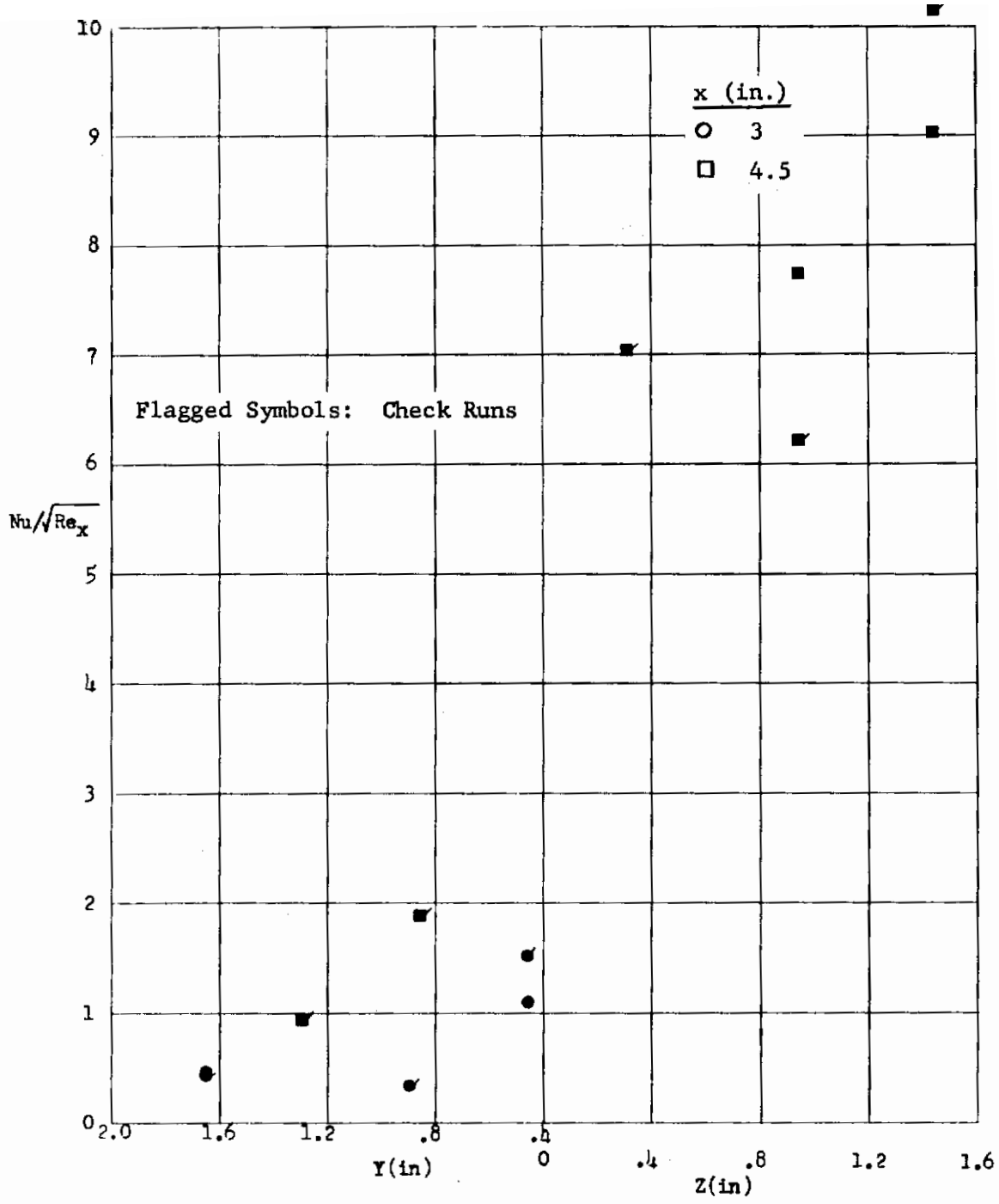

Fig. 30 Wedge Plate Interaction Heat Transfer Data, Large, Sharp LE Wedge, $M_\infty = 13$, $\alpha = 0$

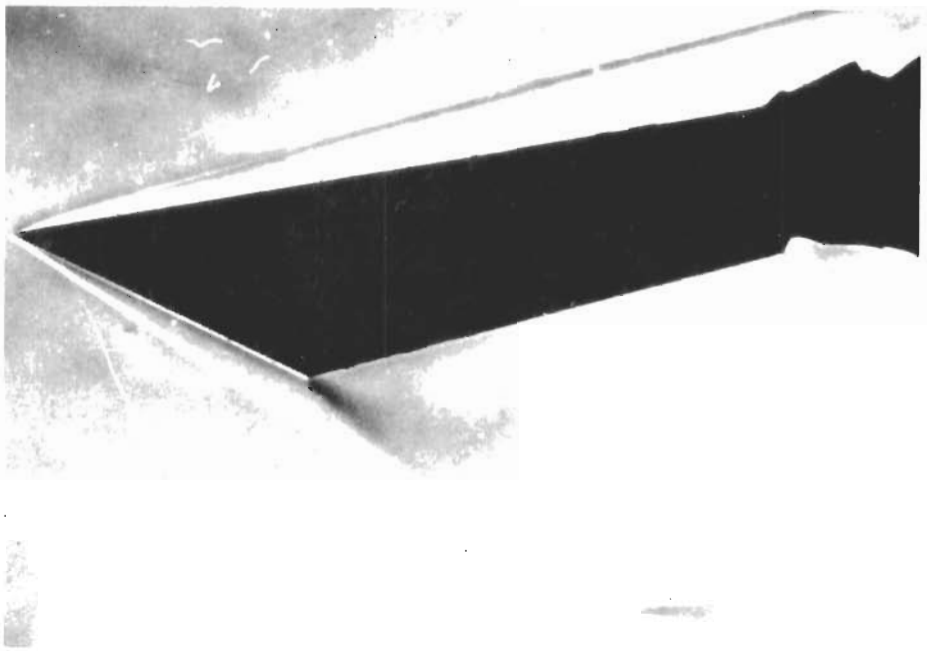

Fig. 31 Schlieren Photograph Showing Model A at Mach 13, $\alpha = +10°$, $\delta = 0$, and $Re/ft = 1.2 \times 10^5$

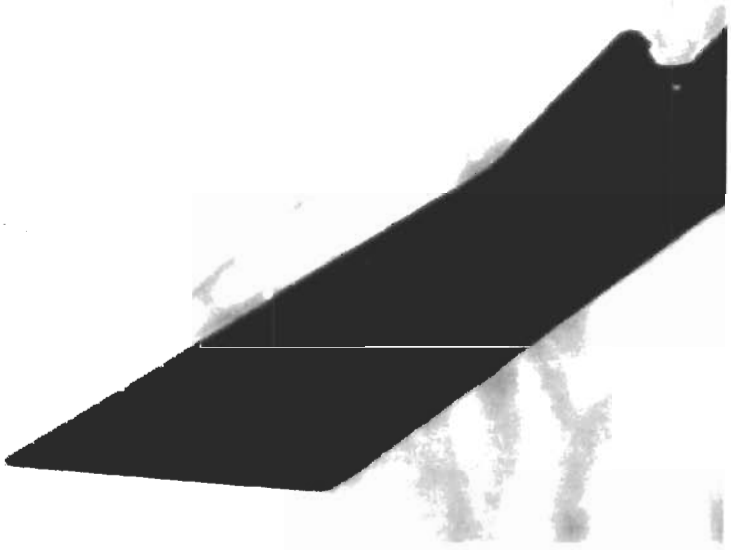

Fig. 32 Schlieren Photograph Showing Model A at Mach 19, $\alpha = +30°$, $\delta = 15°$, and $Re/ft = 0.8 \times 10^5$

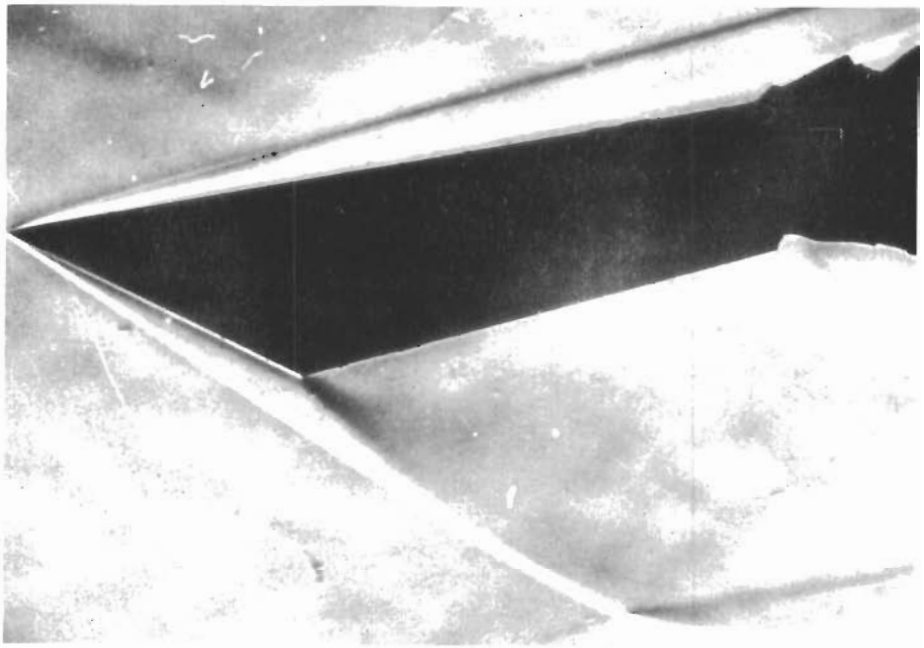

Fig. 31 Schlieren Photograph Showing Model A at Mach 13, $\alpha = +10°$, $\delta = 0$, and $Re/ft = 1.2 \times 10^5$

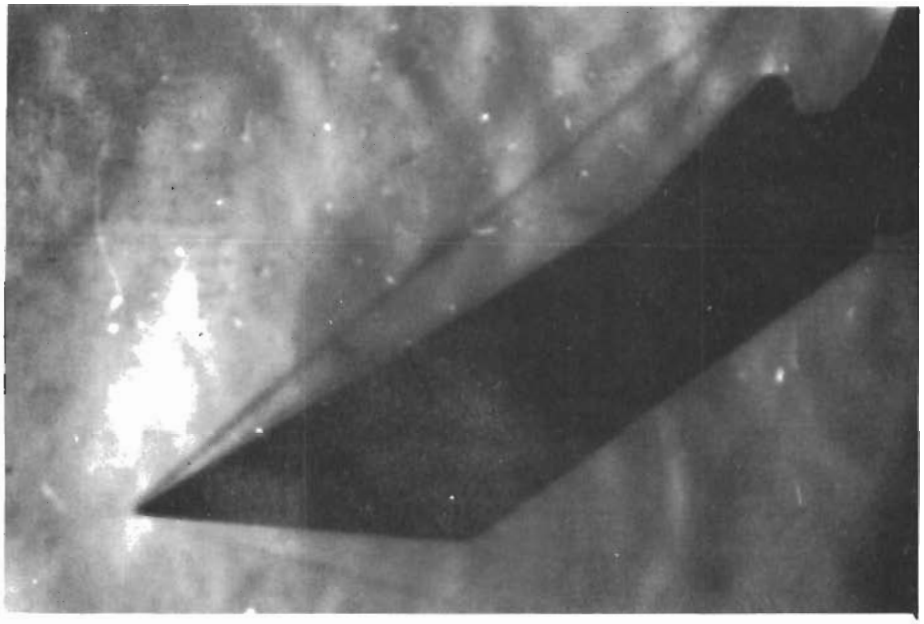

Fig. 32 Schlieren Photograph Showing Model A at Mach 19, $\alpha = +30°$, $\delta = 15°$, and $Re/ft = 0.8 \times 10^5$

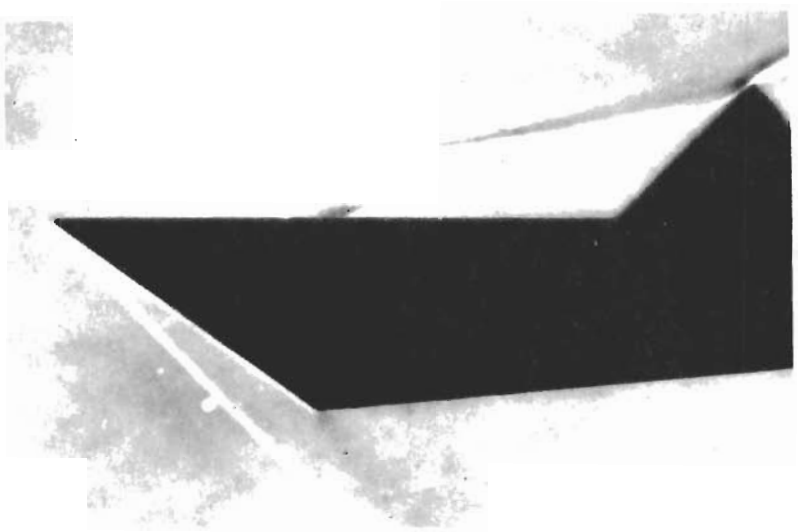

Fig. 33 Schlieren Photograph Showing Model A at Mach 19, $\alpha = 0$, $\delta = 45°$, and Re/ft = 1.3×10^5

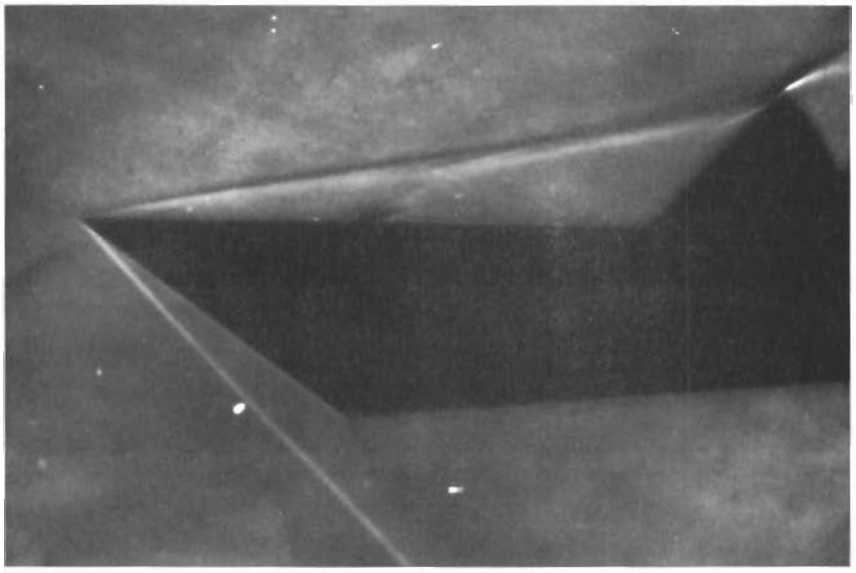

Fig. 33 Schlieren Photograph Showing Model A at Mach 19, $\alpha = 0$, $\delta = 45°$, and Re/ft = 1.3×10^5

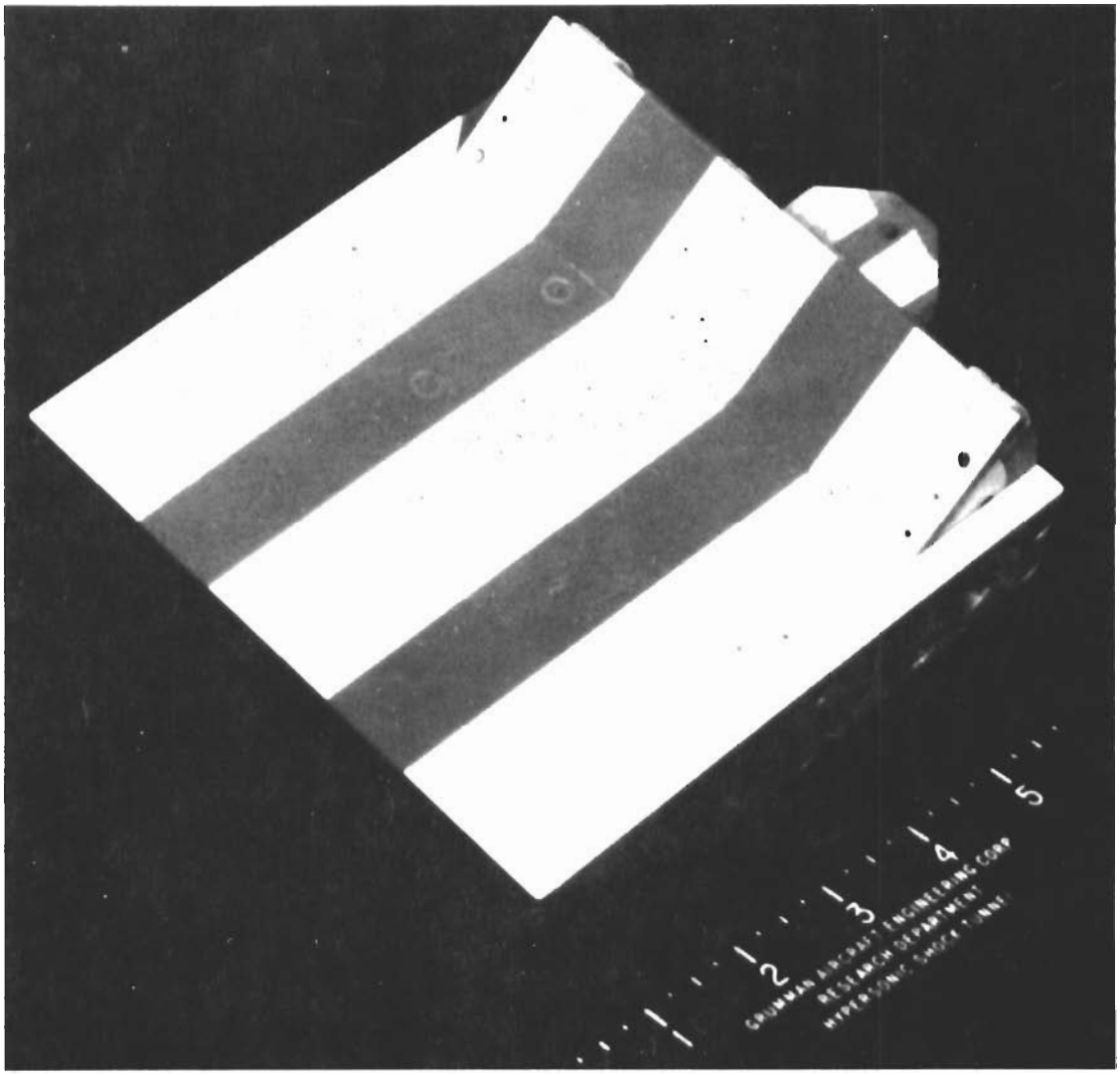

Fig. 34 Experiment with Krylon White: Model A, $\delta = 45°$, Before Run

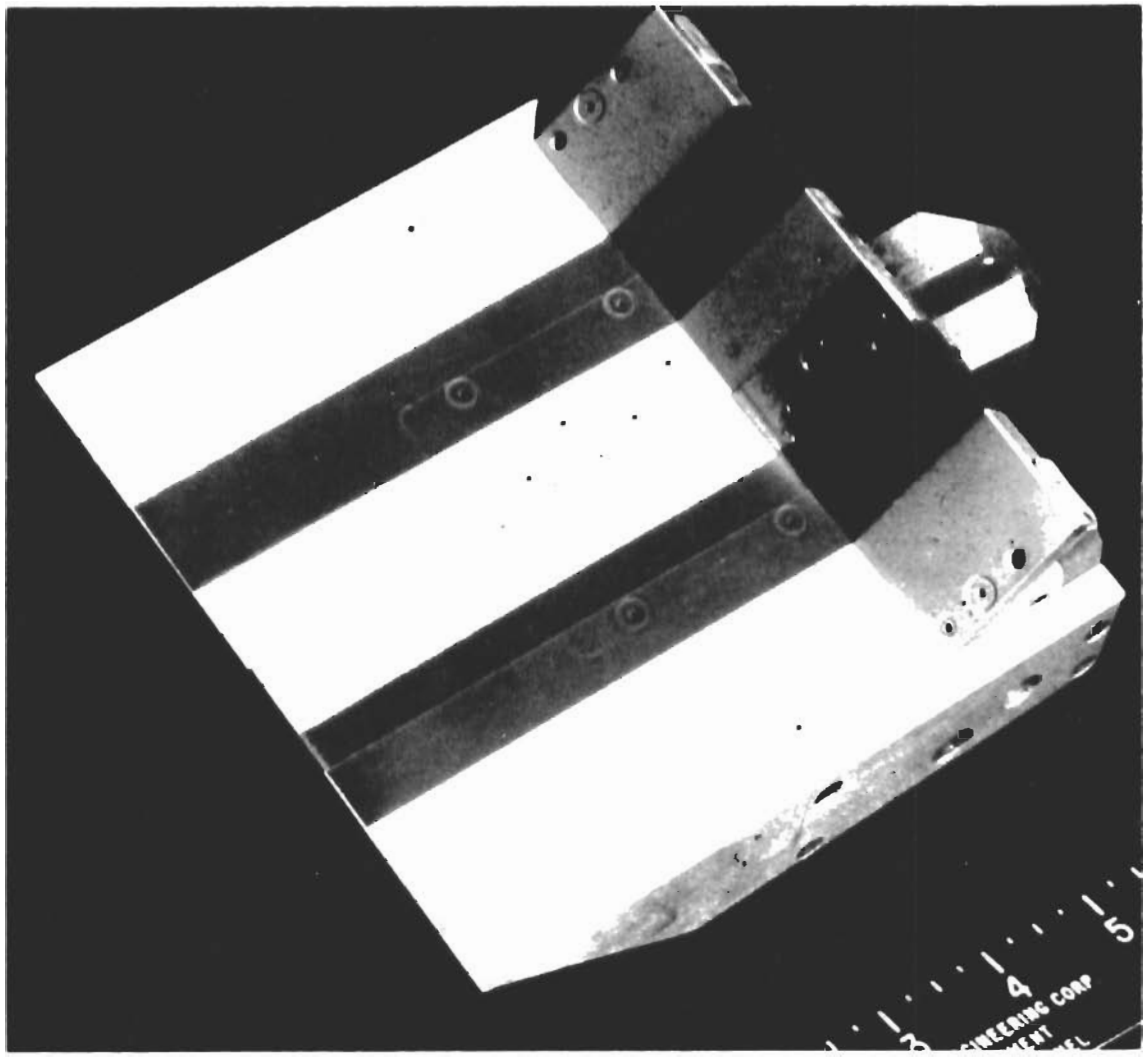

Fig. 35 Experiment with Krylon White: Model A, $\alpha = 0$, $\delta = 45°$, $M_\infty = 19$, and $Re_\infty/ft = 0.8 \times 10^5$

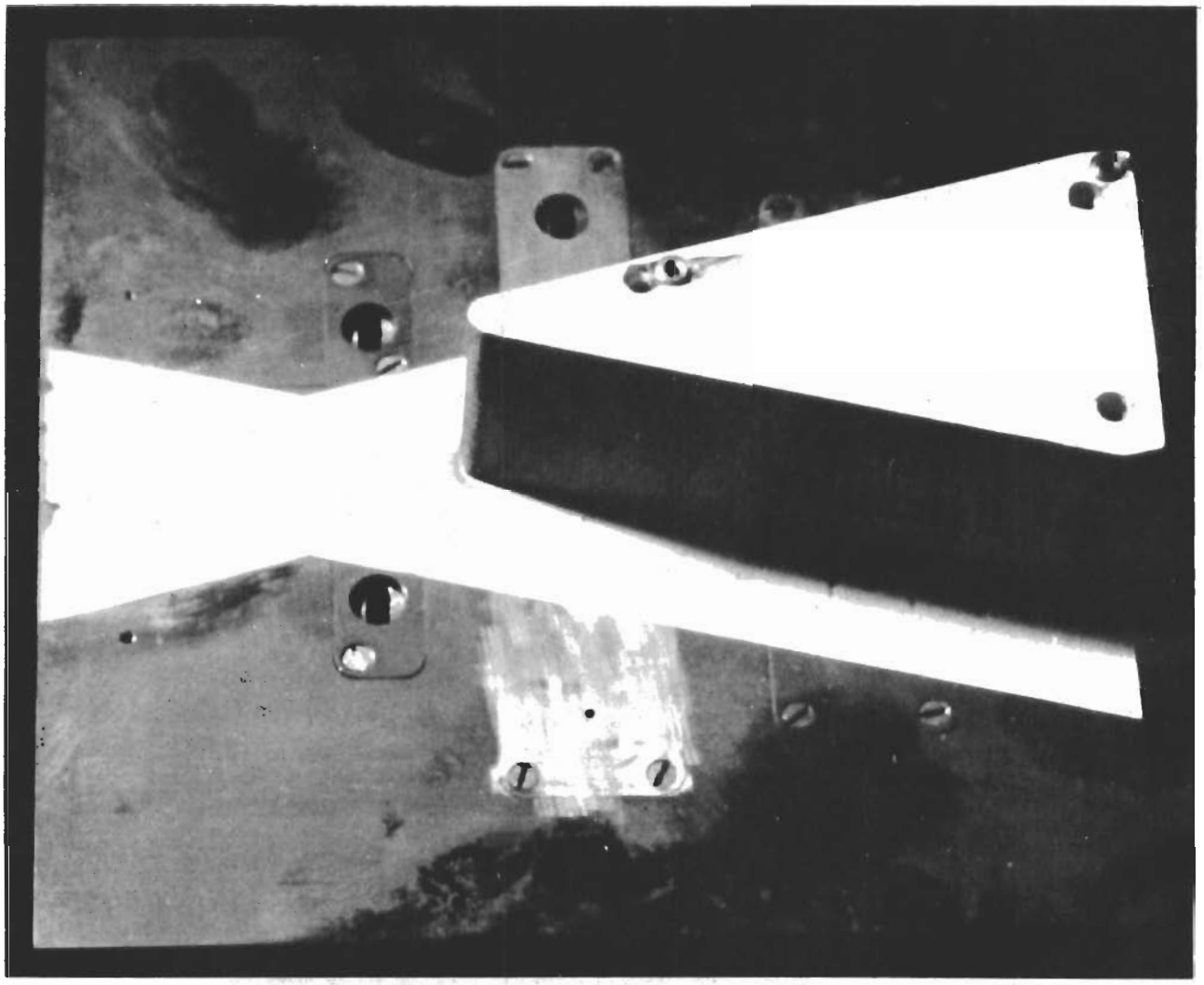

Fig. 36 Experiment with Krylon White: Model B, Large, Blunt LE Wedge, $\alpha = 0$, $M_\infty = 13$, and Re/ft = 0.3×10^5